

Numerical inverse scattering transform for the defocusing nonlinear Schrödinger equation with box-type initial conditions on a nonzero background

A. Gkogkou¹, B. Prinari² and T. Trogdon³

¹Department of Mathematics, Tulane University, New Orleans, 70118-5698, LA, USA.

²Department of Mathematics, University at Buffalo, Buffalo, 14260-2900, NY, USA E-mail: bprinari@buffalo.edu.

³Department of Applied Mathematics, University of Washington, Seattle, 98195-3925, WA, USA.

Keywords: Integrable systems, Riemann-Hilbert problems, nonlinear steepest descent

MSC Codes: *Primary* – 35Q55; *Secondary* – 37K15, 35Q15, 45E05

Abstract

We present a method to solve numerically the Cauchy problem for the defocusing nonlinear Schrödinger (NLS) equation with a box-type initial condition (IC) having a nontrivial background of amplitude $q_o > 0$ as $x \rightarrow \pm\infty$ by implementing numerically the associated Inverse Scattering Transform (IST). The Riemann–Hilbert problem associated to the inverse transform is solved numerically by means of appropriate contour deformations in the complex plane following the numerical implementation of the Deift-Zhou nonlinear steepest descent method. In this work, the box parameters are chosen so that there is no discrete spectrum (i.e., no solitons). In particular, the numerical method is demonstrated to be accurate within the two asymptotic regimes corresponding to two different regions of the (x, t) -plane depending on whether $|x/(2t)| < q_o$ or $|x/(2t)| > q_o$, as $t \rightarrow \infty$.

1. Introduction

In this work, we present a method to numerically solve the Cauchy problem for the defocusing nonlinear Schrödinger (NLS) equation:

$$iq_t + q_{xx} + 2(q_o^2 - |q|^2)q = 0, \quad (1.1)$$

on a nonzero background, and specifically with the following constant nonzero boundary conditions at infinity

$$\lim_{x \rightarrow \pm\infty} q(x, t) = q_{\pm} = q_o e^{i\theta_{\pm}}, \quad q_o > 0, \theta_{\pm} \in \mathbb{R}. \quad (1.2)$$

Note that due to the phase invariance of the NLS equation (1.1), in the following we will set $\theta_+ = -\theta_- = \theta$ without loss of generality. Note also that the additional linear term in (1.1), compared to the standard form of the equation when $q_o = 0$, can be removed by a gauge transformation $q \rightarrow e^{2iq_o^2 t} q$, and has simply the effect of ensuring that the boundary conditions (1.2) are time-independent.

As it is well-known, the NLS equation is a completely integrable system, which implies that it admits a Lax pair (an overdetermined system of ODEs whose compatibility condition is equivalent to the integrable PDE), and its Cauchy problem can be solved by means of the Inverse Scattering Transform (IST), a nonlinear analog of the Fourier transform. Similarly to the case of linear PDEs, the solution of the Cauchy problem by IST proceeds in three steps: (i) Direct problem - the transformation of the initial data from the original “physical” variables $(q(x, 0))$, to the transformed “scattering” variables $S(k, 0)$ (reflection coefficient, discrete eigenvalues and norming constants); (ii) Time dependence - the

evolution of the scattering data, i.e., finding $\mathcal{S}(k, t)$; (iii) Inverse problem - the recovery of the evolved solution $q(x, t)$ from the evolved solution in the transformed variables $\mathcal{S}(k, t)$. The eigenfunctions of the first operator in the Lax pair, referred to as the “scattering problem”, play a crucial role in the theory: the direct problem involves integral equations for the eigenfunctions, through which the scattering data are defined; the inverse problem can be formulated in terms of a Riemann-Hilbert problem (RHP) for the eigenfunctions, from which one then reconstructs the solution of the nonlinear PDE. Furthermore, the inverse problem reveals that the solitons are the portion of the solution associated with the discrete spectrum (discrete eigenvalues and related norming constants).

Although the IST has been around for over 60 years, its numerical implementation is a relatively recent effort. The numerical IST has been implemented in the literature for a number of nonlinear integrable equations: Korteweg-de Vries and modified Korteweg-de Vries equations [33, 29], focusing and defocusing NLS equations [31], and the Toda lattice [4], in all cases under the assumption that the initial condition (IC) is rapidly decaying as $|x| \rightarrow \infty$ (typically, in Schwartz class). For non-decaying ICs for the Korteweg-de Vries equation see [3, 2]. As the previous works already showed, the main advantage of the numerical IST over direct numerical simulations is that the computational cost to approximate the solution at given values of x, t can be independent of x and t , while the computational cost using time-stepping methods grows rapidly in time, thus making traditional numerical methods inefficient to capture the solution for large times. This is particularly problematic for the NLS equations, both focusing and defocusing, due to the presence of an oscillatory dispersive tail.

In the present work, we will consider for the numerical implementation of the IST a piecewise constant initial condition of box-type, i.e.,

$$q(x, 0) = \begin{cases} q_- = q_o e^{-i\theta}, & x < -L \\ q_c = h e^{i\alpha}, & -L < x < L \\ q_+ = q_o e^{i\theta}, & x > L \end{cases} \quad (1.3)$$

where h, q_o and L are arbitrary non-negative parameters and θ and α are arbitrary phases. Furthermore, we will restrict ourselves to values of the box parameters for which no discrete eigenvalues (i.e., no solitons) are present. The rationale for restricting to a piecewise constant IC such as above is the following: To begin with, for these types of ICs one can explicitly compute the scattering data (following, e.g., [5]), which greatly simplifies the numerical implementation of the direct problem. Furthermore, for the inverse problem, the chosen IC yields analyticity of the reflection coefficient, which will avoid the need for a $\bar{\partial}$ -problem when the associated Riemann-Hilbert problem is deformed. Moreover, having at our disposal the explicit expression of the reflection coefficient allows us to perform consistency checks and better control the convergence of the numerical integrations. Finally, discontinuous ICs are also notoriously much more difficult to handle from the point of view of direct numerical simulations, thus showcasing the advantages of a numerical IST over traditional time-stepping methods [18, 23]. On the other hand, the discontinuous IC results in slower asymptotic decay of the reflection coefficient, which will require a more careful handling of the numerical integrations involved in the solution of the inverse problem.

To elaborate on numerical challenges, we note that the most common approach to numerical approximations of solutions of whole-like PDE problems is using a periodic approximation with a large period. This allows one to use efficient Fourier methods and the technology of exponential integrators [21, 22]. But for discontinuous data one is necessarily combatting classical Gibbs phenomenon while simultaneously trying to resolve the nonlinear Gibbs phenomenon that is present in the true solution [16]. To compare the numerical IST approach with classical approaches, we incorporated the artificially damping/filtering of [23] and still needed a period of length 800 and over a million Fourier modes to achieve an approximation accurate to within an error 10^{-3} at $t = 1$. The runtime of such a simulation on a laptop is likely to be on the order of hours, in contrast to the method we propose here that requires a matter of seconds to evaluate the solution at a point in the (x, t) plane (see, for example, the plot in Fig. 1).

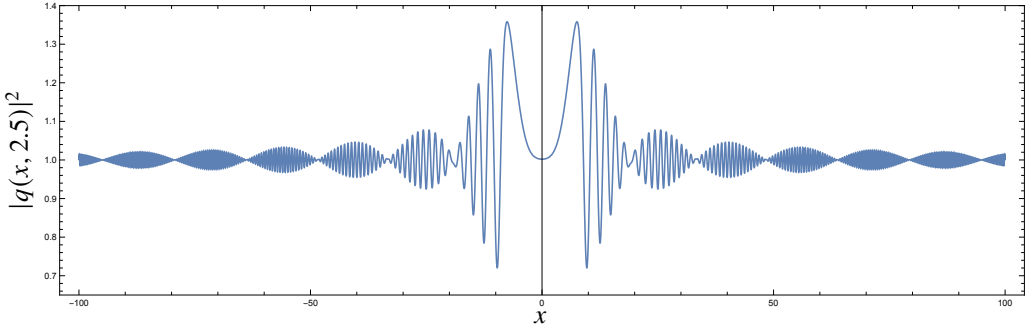


Figure 1: The squared modulus of the solution of the NLS equation with IC (1.3) at $t = 2.5$ with box parameters as in (3.18).

From a theoretical point of view, one of the challenges of dealing with a constant, nonzero background (here, $q_o > 0$) in the IST is the fact that the asymptotic eigenvalues and eigenfunctions have branching in the spectral plane, originating from $\lambda = \sqrt{k^2 - q_o^2}$. The IST can be carried out by introducing an appropriate branch cut in the complex k -plane, and this is also the framework adopted in [1] for their “robust” IST for the focusing NLS equation. For our numerical implementation, we will take advantage of the formulation of the IST in terms of the uniformization variable $z = k + \lambda$, for which $k = (z + q_o^2/z)/2$ and $\lambda = (z - q_o^2/z)/2$, and which allows the direct and inverse problems to be formulated in the entire complex z -plane and avoid branching altogether. The uniform variable was first introduced by Faddeev and Takhtajan in [17], and since then it has been successfully utilized in a large number of papers dealing with the IST of scalar, vector and matrix NLS equations on a nontrivial, symmetric background. This is also the approach used in [6] and [37], where the Deift-Zhou nonlinear steepest descent method was employed to compute the long-time asymptotic behavior of solutions of the defocusing NLS. According to the results in [6, 37], there are two different asymptotic regions, which require different contour deformations in the associated oscillatory RHP for the eigenfunctions, depending on whether $|\xi| = |x/(2t)| < 1$ (the so-called “solitonic region”, where the phase function in the RHP has no stationary points), and $|\xi| > 1$ (the “solitonless” region, where the phase function exhibits 2 real stationary points). The long-time asymptotics problem in the solitonic region has been studied in [6], while [37] investigated the long-time asymptotics in the solitonless region.

The numerical IST scheme for the solution of the inverse problem has two major components: the first is the use of a Chebyshev collocation method for solving RHPs (as in the case of rapidly decaying ICs dealt with in [33, 29, 31], see [27, 32] for an overview of the framework), and the second is contour deformation in the complex plane, which mimics the corresponding deformations used for estimating the long-time asymptotics in [6, 37]. Once the proper contour deformations are implemented numerically, one has to handle the numerical computation of three different Cauchy-type integrals, featuring: (i) integrands with slow decay at infinity (due to the discontinuous IC); (ii) integrands with rapid oscillations at $z = 0$ (introduced by the uniform variable, since $k \rightarrow \infty$ on one of the two sheets of the Riemann surface is mapped onto $z = 0$); (iii) integrands with a logarithmic singularity at $z = \pm q_o$ (these singularities depend on the symmetries of the reflection coefficient, and are present also with a smooth IC, see [6]). For the first two integrals, we can simply judiciously truncate the integration domains to achieve good accuracy while still keeping the computational costs at bay. As to the last integrals, we generalize the contour deformation used to address the analogous problem for the Toda lattice [4], and reduce each integral to one that can be analytically computed.

The plan of the paper is as follows. In Sec 2 we give a succinct overview of the IST for the defocusing NLS equation formulated in terms of the uniform variable z for a general IC with symmetric nonzero boundary conditions (1.2) as $|x| \rightarrow \infty$. We will assume $q(x, t)$ to be decaying to the boundary conditions sufficiently rapidly, specifically in analogy with the function class considered in [6]. In Sec 3, we first

show how one can remove the singularity of the RHP at $z = 0$, and then we discuss the jump matrix factorizations and contour deformations that will be utilized for the numerical solution of the RHP in the solitonic and solitonless regions (Sec 3.4 and Sec 3.5, respectively). Sec 4 provides the details of the numerical implementation of the RHP and its solution for a box-type IC of the form (1.3) with box parameters chosen to ensure absence of discrete eigenvalues/solitons, and hence of poles in the RHP, via the routine `RHSolve` (a Mathematica implementation of the code will be available as electronic supplementary material). In turn, the numerical solution of the RHP at any given (x, t) is then used to obtain the approximation for $q(x, t)$, and some plots illustrating the solution at various times are provided. The accuracy of the numerical code is verified by substituting the computed $q(x, t)$ into the defocusing NLS equation using a second-order finite difference scheme in both time and space. Finally, Sec 5 is devoted to some concluding remarks.

The generalization of this work to an arbitrary smooth IC decaying sufficiently rapidly to a symmetric nonzero background as $|x| \rightarrow \infty$ will be the subject of future investigation. We anticipate that the numerical implementation of the direct problem, required for a general IC, will not pose any particular challenge, as it can be done similarly to the case of rapidly decaying ICs. For data with some degree of exponential decay, the deformations outlined here will likely apply for the inverse problem, indicating that indeed, the methodology presented here paves the way for these future implementations.

2. Overview of the IST

In this section we provide a review of the IST for the defocusing NLS equation on a nonzero symmetric background.

2.1. Integrability and Jost eigenfunctions

Equation (1.1) is an integrable system and admits the following Lax pair

$$\Phi_x = \mathbf{X}\Phi, \quad \Phi_t = \mathbf{T}\Phi, \quad (2.1a)$$

$$\mathbf{X}(x, t; k) = -ik\sigma_3 + Q, \quad \mathbf{T}(x, t; k) = -2ik^2\sigma_3 + i\sigma_3(Q_x - Q^2 + q_o^2 I_2) + 2kQ, \quad (2.1b)$$

$$Q(x, t) = \begin{pmatrix} 0 & q(x, t) \\ q^*(x, t) & 0 \end{pmatrix}, \quad \sigma_1 = \begin{pmatrix} 0 & 1 \\ 1 & 0 \end{pmatrix}, \quad \sigma_2 = \begin{pmatrix} 0 & -i \\ i & 0 \end{pmatrix}, \quad \sigma_3 = \begin{pmatrix} 1 & 0 \\ 0 & -1 \end{pmatrix}. \quad (2.1c)$$

Here and in the following, $*$ denotes complex conjugation, and σ_j for $j = 1, 2, 3$ are the usual Pauli matrices. For the purpose of reviewing the IST on a nonzero background, we will assume the IC to be in the analog functional class as in [6]. Specifically, we introduce

$$\tilde{q}(x) = q_o [\cos \theta + i \sin \theta \tanh x] \quad (2.2)$$

to generalize $\tanh x$ in [6] to a smooth function which approaches, at exponential rates, the boundary conditions (1.2). We consider the weighted spaces $L^{p,s}(\mathbb{R})$ with norm defined as

$$\|f\|_{L^{p,s}(\mathbb{R})} := \left(\int_{\mathbb{R}} \langle x \rangle^{2s} |f(x)|^p dx \right)^{1/p} \quad \langle x \rangle := \sqrt{1+x^2} \quad (2.3)$$

(note that $2s = q$, compared to [6]), as well as the Sobolev spaces

$$H^\ell(\mathbb{R}) = \left\{ f : \mathbb{R} \rightarrow \mathbb{C} : f^{(k)} \in L^2(\mathbb{R}) \text{ for } k = 0, \dots, \ell \right\} \quad (2.4)$$

and

$$H^{1,\ell}(\mathbb{R}) := L^{2,\ell}(\mathbb{R}) \cap H^\ell(\mathbb{R}), \quad (2.5)$$

where the L^2 -Sobolev bijectivity of the IST for the focusing NLS equation was established in the case of rapidly decaying ICs [38]. Then, combining results from [19, 20, 14, 6], we will assume the IC such that $q(x, 0) - \tilde{q}(x) \in H^{1,\ell}(\mathbb{R})$ for $\ell = 1, 3/2, 2$ (these are the same as the spaces Σ_m in [6] with $m = 2, 3, 4$, respectively), and highlight the corresponding implications on the IST as it becomes relevant.

The Jost eigenfunctions Φ_{\pm} are defined as simultaneous solutions of the two linear equations of the Lax pair with boundary conditions

$$\Phi_{\pm}(x, t; k) \sim [Y_{\pm}(k) + o(1)] e^{i\Omega(x,t;k)\sigma_3}, \quad x \rightarrow \pm\infty, \quad (2.6a)$$

$$\Omega(x, k; t) = -\lambda x - 2k\lambda t, \quad \lambda^2 = k^2 - q_o^2, \quad (2.6b)$$

$$Y_{\pm}(k) = I_2 - \frac{i}{k + \lambda} \sigma_3 Q_{\pm}, \quad Q_{\pm} = \begin{pmatrix} 0 & q_{\pm} \\ q_{\pm}^* & 0 \end{pmatrix}. \quad (2.6c)$$

Note that in the expression for Ω above the second term has the opposite sign compared to [5, 6, 37]. This small typo does not affect in any significant way the results in those papers, but it switches the regions with $t > 0$ and those with $t < 0$. For convenience, we introduce the uniformization variable z defined by the conformal mapping

$$z = k + \lambda \quad (2.7)$$

which is inverted via the relations

$$k(z) = \frac{1}{2} \left(z + q_o^2/z \right), \quad \lambda(z) = \frac{1}{2} \left(z - q_o^2/z \right). \quad (2.8)$$

The asymptotic behavior of the eigenfunctions now becomes

$$\Phi_{\pm}(x, t; z) \sim [Y_{\pm}(z) + o(1)] e^{i\Omega(x,t;z)\sigma_3}, \quad x \rightarrow \pm\infty, \quad (2.9a)$$

$$Y_{\pm}(z) = \begin{pmatrix} 1 & -\frac{i}{z} q_{\pm} \\ \frac{i}{z} q_{\pm}^* & 1 \end{pmatrix} = \begin{pmatrix} 1 & -\frac{i}{z} q_o e^{\pm i\theta} \\ \frac{i}{z} q_o e^{\mp i\theta} & 1 \end{pmatrix}. \quad (2.9b)$$

As usual, it is more convenient to introduce modified eigenfunctions

$$M_{\pm}(x, t; z) = \Phi_{\pm}(x, t; z) e^{-i\Omega(x,t;z)\sigma_3} \quad (2.10)$$

which satisfy the boundary conditions

$$M_{\pm}(x, t; z) \sim Y_{\pm}(z) + o(1), \quad x \rightarrow \pm\infty. \quad (2.11)$$

If the IC $q(x, 0)$ is such that $q(x, 0) - \tilde{q}(x) \in H^{1,1}(\mathbb{R})$, then the modified eigenfunctions $M_{-,1}(x, t; z)$, $M_{+,2}(x, t; z)$ are analytic in the upper half-plane of z and continuous up to $\mathbb{R} \setminus \{0\}$, while $M_{-,2}(x, t; z)$, $M_{+,1}(x, t; z)$ are analytic in the lower half-plane of z and continuous up to $\mathbb{R} \setminus \{0\}$ (see [14, 6]). Here and in the following, the additional subscript $j = 1, 2$ in M_{\pm} denotes the corresponding column of the matrix function. Furthermore, the following lemma holds.

Lemma 1. *The modified eigenfunctions M_{\pm} satisfy the symmetries*

$$M_{\pm}^*(z^*) = \sigma_1 M_{\pm}(z) \sigma_1, \quad M_{\pm} \left(q_o^2/z \right) = \frac{z}{q_o} M_{\pm}(z) \sigma_2 e^{\mp i\theta\sigma_3} \quad (2.12)$$

for any $q_o > 0$ and $\theta \in \mathbb{R}$.

Proof. Using the symmetries of the Lax pair

$$\mathbf{X}^*(x, t; z^*) = \sigma_1 \mathbf{X}(x, t; z) \sigma_1, \quad \mathbf{X} \left(x, t; q_o^2/z \right) = \mathbf{X}(x, t; z) \quad (2.13a)$$

$$\mathbf{T}^*(x, t; z^*) = \sigma_1 \mathbf{T}(x, t; z) \sigma_1, \quad \mathbf{T}\left(x, t; q_o^2/z\right) = \mathbf{T}(x, t; z) \quad (2.13b)$$

and the asymptotics of Φ_{\pm} as $x \rightarrow \pm\infty$, one can show that Φ_{\pm} satisfy the symmetries

$$\Phi_{\pm}^*(z^*) = \sigma_1 \Phi_{\pm}(z) \sigma_1, \quad \Phi_{\pm}\left(q_o^2/z\right) = \frac{z}{q_o} \Phi_{\pm}(z) \sigma_2 e^{\mp i\theta\sigma_3}. \quad (2.14)$$

Symmetries (2.12) follow directly from equation (2.10) and the symmetries of the function Ω , namely

$$\Omega(x, t; z^*) = \Omega(x, t; z), \quad \Omega\left(x, t; q_o^2/z\right) = -\Omega(x, t; z). \quad (2.15)$$

□

2.2. Direct problem: scattering data

The Jost eigenfunctions Φ_{\pm} are two fundamental solutions of the Lax pair for any $z \in \mathbb{R} \setminus \{\pm q_o\}$, since

$$\det \Phi_{\pm}(x, t, z) \equiv \det Y_{\pm}(z) = 1 - q_o^2 z^{-2}. \quad (2.16)$$

Therefore, there exists a 2×2 scattering matrix $S(z)$ (independent of x, t) such that

$$\Phi_{-}(x, t, z) = \Phi_{+}(x, t, z) S(z), \quad S(z) = \begin{pmatrix} a(z) & b^*(z) \\ b(z) & a^*(z) \end{pmatrix}, \quad z \in \mathbb{R} \setminus \{\pm q_o\}. \quad (2.17)$$

The time independence of the scattering matrix $S(z)$ is a consequence of having defined the Jost eigenfunctions as simultaneous solutions of the Lax pair, not just of the scattering problem. After replacing the modified eigenfunctions, the last equation becomes

$$M_{-,1}(x, t, z)/a(z) = M_{+,1}(x, t, z) + \rho(z) M_{+,2}(x, t, z) e^{-2i\Omega(x, t, z)}, \quad (2.18a)$$

$$M_{-,2}(x, t, z)/a^*(z) = M_{+,2}(x, t, z) + \rho^*(z) M_{+,1}(x, t, z) e^{2i\Omega(x, t, z)}, \quad (2.18b)$$

where we introduced the reflection coefficient

$$\rho(z) = b(z)/a(z). \quad (2.19)$$

Equation (2.16), combined with (2.17), yields the following expressions for the scattering coefficients:

$$a(z) = \frac{1}{1 - q_o^2 z^{-2}} \det(M_{-,1}(z), M_{+,2}(z)), \quad b(z) = \frac{1}{1 - q_o^2 z^{-2}} \det(M_{+,1}(z), M_{-,1}(z)) \quad (2.20)$$

where we have omitted the (x, t) dependence in the right-hand side for brevity. The above expressions show that even if the Jost eigenfunctions are continuous at $z = \pm q_o$, in general the scattering coefficients are singular at those points.

Discrete eigenvalues are the zeros of the scattering coefficient $a(z)$ in \mathbb{C}^+ and their complex conjugates (as zeros of $a^*(z^*)$) in \mathbb{C}^- . Such zeros are known to be simple, and located on the circle of radius q_o due to the self-adjointness of the scattering problem [17]. Note that the only possible discrete eigenvalues embedded in the continuous spectrum, i.e., on the real z -axis, are $\pm q_o$. In [14] it is shown that if $q(x, 0) - q_{\pm} \in L^{1,2}(\mathbb{R}^{\pm})$, then $a(z)$ does not vanish at $\pm q_o$. Moreover, Eqs. (2.20) imply that at each pair of discrete eigenvalues z_j, z_j^* :

$$M_{-,1}(x, t, z_j) = b_j M_{+,2}(x, t, z_j) e^{-2i\Omega(x, t, z_j)}, \quad M_{-,2}(x, t, z_j^*) = b_j^* M_{+,1}(x, t, z_j^*) e^{2i\Omega(x, t, z_j^*)} \quad (2.21)$$

for some $b_j \in \mathbb{C}$. Additional smoothness and decay properties of the reflection coefficient are established in [6] under suitable assumptions on the IC. Specifically:

- If $q(x, 0) - \tilde{q}(x) \in H^{1,1}(\mathbb{R})$, then $\rho \in L^2(\mathbb{R})$ and $\|\log(1 - |\rho|^2)\|_{L^p} < \infty$ for all $p \geq 1$;
- If $q(x, 0) - \tilde{q}(x) \in H^{1,3/2}(\mathbb{R})$, then $\rho \in H^1(\mathbb{R})$ and moreover the discrete eigenvalues are necessarily finite in number.

Even though it will not be relevant for the present work, we mention that in [6] it was also shown that requiring $q(x, 0) - \tilde{q}(x) \in H^{1,2}(\mathbb{R})$ allows to obtain bounds of the $\bar{\partial}$ -derivatives of the reflection coefficient which were there used for the long-time estimates in the inverse problem.

For completeness, we include the symmetries of the scattering data in the following proposition, whose proof follows straightforwardly from the symmetries (2.14) of the Jost eigenfunctions.

Lemma 2. *The scattering matrix $S(z)$ satisfies*

$$S(q_o^2/z) = e^{i\theta\sigma_3} \sigma_2 S(z) \sigma_2 e^{i\theta\sigma_3} \quad \forall z \in \mathbb{R} \setminus \{\pm q_o\}. \quad (2.22)$$

Consequently, one has

$$a(q_o^2/z) = e^{2i\theta} a^*(z^*), \quad z \in \mathbb{C}^+ \quad (2.23a)$$

$$b(q_o^2/z) = -b^*(z), \quad \rho(q_o^2/z) = -e^{-2i\theta} \rho^*(z), \quad z \in \mathbb{R} \setminus \{\pm q_o\}. \quad (2.23b)$$

Moreover, the proportionality constants b_j defined in (2.21) satisfy

$$b_j^* = -b_j. \quad (2.24)$$

We emphasize that with a piecewise IC, the direct problem of the IST can be solved exactly. Specifically, as shown in [5], for any piecewise IC (1.3), one can derive an explicit expression for the scattering data by expressing at the boundary of each region, the (fundamental) solution on the left as a linear combination of the (fundamental) solution on the right, and obtain:

$$a(z) = \frac{1}{\lambda(z)\mu(z)} e^{i(2L\lambda(z)+\theta)} \left\{ \mu(z) \cos(2L\mu(z)) [\lambda(z) \cos \theta - ik(z) \sin \theta] \right. \\ \left. + i \sin(2L\mu(z)) [hq_o \cos \alpha - k(z)(k(z) \cos \theta - i\lambda(z) \sin \theta)] \right\} \quad (2.25a)$$

$$b(z) = \frac{1}{\lambda(z)\mu(z)} \left\{ -q_o \mu(z) \sin \theta \cos(2L\mu(z)) \right. \\ \left. + [hk(z) \cos \alpha - k(z)q_o \cos \theta - ih\lambda(z) \sin \alpha] \sin(2L\mu(z)) \right\}, \quad (2.25b)$$

where

$$k(z) = \frac{1}{2}(z + q_o^2/z), \quad \lambda(z) = \sqrt{k(z)^2 - q_o^2} \equiv \frac{1}{2}(z^2 - q_o^2/z), \quad \mu(z) = \sqrt{k(z)^2 - h^2}. \quad (2.26)$$

It is important to point out that although $\mu(z)$ is defined in terms of a square root, there is no branching in the IST. Indeed, μ does not enter in the definition of the Jost eigenfunctions, and (2.25) show that only even functions of μ appear in the scattering coefficients, which are therefore independent of the choice of sign of the square root.

2.3. Asymptotic behavior of eigenfunctions and scattering data

To formulate the inverse problem properly, one needs to determine the asymptotic behavior of eigenfunctions and scattering data as $z \rightarrow 0$, $z \rightarrow \infty$ and as $z \rightarrow \pm q_0$. Specifically, the asymptotic behavior of the eigenfunctions is obtained from appropriate Volterra integral equations for the eigenfunction (cf., e.g., [14]), and it is given by:

$$M_{\pm}(x, t, z) = \begin{pmatrix} 1 + iI_0(x, t)/z & -iq(x, t)/z \\ iq^*(x, t)/z & 1 - iI_0(x, t)/z \end{pmatrix} + O(z^{-2}), \quad z \rightarrow \infty, \quad (2.27a)$$

$$M_{\pm}(x, t, z) = \begin{pmatrix} q(x, t)/q_{\pm} & I_0(x, t)/q_{\pm} - iq_{\pm}/z \\ I_0(x, t)/q_{\pm} + iq_{\pm}^*/z & q^*(x, t)/q_{\pm}^* \end{pmatrix} + O(z^2), \quad z \rightarrow 0, \quad (2.27b)$$

where

$$I_0(x, t) = \int_x^{+\infty} (|q(x', t)|^2 - q_0^2) dx'. \quad (2.28)$$

Combining Eqs. (2.20) and (2.27) one can also derive the asymptotic behavior of the scattering data

$$a(z) = 1 + O(z^{-2}), \quad b(z) = O(z^{-2}), \quad \rho(z) = O(z^{-2}) \quad z \rightarrow \infty, \quad (2.29a)$$

$$a(z) = q_+/q_- + O(z^2), \quad b(z) = O(z^2), \quad \rho(z) = O(z^2), \quad z \rightarrow 0. \quad (2.29b)$$

For ICs in $\tilde{q}(x) + H^{1,1}(\mathbb{R})$ the modified eigenfunctions are continuous at $z = \pm q_0$, and Eqs. (2.20) show that generically the scattering data have simple poles at $\pm q_0$:

$$a(z) = \frac{\alpha_{\pm}}{z \mp q_0} + O(1), \quad b(z) = \mp \frac{\alpha_{\pm}}{z \mp q_0} + O(1), \quad (2.30)$$

where $\alpha_{\pm} = \det(M_{-,1}(x, t, \pm q_0), M_{+,2}(x, t, \pm q_0))$ [and $\alpha_{\pm} \neq 0$ unless the columns of M_{\pm} become linearly dependent at either $z = q_0$ or $z = -q_0$ or both, in which case the points $\pm q_0$ are called ‘‘virtual levels’’]. Note that the reflection coefficient is always bounded at $z = \pm q_0$, and in particular

$$\rho(\pm q_0) = \mp i e^{-i\theta}. \quad (2.31)$$

2.4. Inverse problem: Riemann-Hilbert formulation

Within the IST framework, the inverse problem amounts to reconstructing the Jost eigenfunctions in terms of the scattering data, from which one can then recover $q(x, t)$ for any $t > 0$. For this purpose, we introduce:

$$m(z) := m(x, t, z) = \begin{cases} \left(M_{-,1}(x, t, z)/a(z), & M_{+,2}(x, t, z) \right), & z \in \mathbb{C}^+ \\ \left(M_{+,1}(x, t, z), & M_{-,2}(x, t, z)/a^*(z^*) \right), & z \in \mathbb{C}^- \end{cases} \quad (2.32)$$

For a generic IC, the problem might support solitons that arise from the zeros of $a(z)$ in \mathbb{C}^+ , and their complex conjugates, zeros of $a^*(z^*)$ in \mathbb{C}^- . Let $N \in \mathbb{N}$ denote the number of solitons (necessarily finite for IC in $\tilde{q}(x) + H^{1,3/2}(\mathbb{R})$, as mentioned above), which implies that m has N poles in \mathbb{C}^+ with their complex conjugates appearing as poles in \mathbb{C}^- . The properties established for the eigenfunctions and the scattering coefficient $a(z)$ in the direct problem then yield the following RHP for m .

RHP 1 (RHP for m with solitons). *Find a 2×2 matrix-valued function m such that:*

1. m is sectionally analytic in $\mathbb{C} \setminus \mathbb{R}$

2. The non-tangential limits $m_{\pm}(x, t, z) = \lim_{\substack{\zeta \rightarrow z \\ \zeta \in \mathbb{C}^{\pm}}} m_{\pm}(x, t, \zeta)$ exist for any $z \in \mathbb{R} \setminus \{0\}$ and satisfy the following jump relation across the real axis:

$$m_+(z) = m_-(z)G_m(x, t, z), \quad G_m(x, t, z) = \begin{pmatrix} 1 - |\rho(z)|^2 & -\rho^*(z)e^{2i\Omega(x, t, z)} \\ \rho(z)e^{-2i\Omega(x, t, z)} & 1 \end{pmatrix},$$

$$\Omega(x, t, z) = -\lambda(z)x - 2k(z)\lambda(z)t \quad (2.33)$$

3. m has simple poles at $\{z_j\}_{j=1}^N$ in \mathbb{C}^+ and $\{z_j^*\}_{j=1}^N$ in \mathbb{C}^- with $|z_j| = q_o$ for all $j = 1, \dots, N$, and with residue conditions:

$$\text{Res}_{z=z_j} m(z) = \lim_{z \rightarrow z_j} m(z) \begin{pmatrix} 0 & 0 \\ C_j e^{-2i\Omega(x, t, z_j)} & 0 \end{pmatrix} \quad (2.34a)$$

$$\text{Res}_{z=z_j^*} m(z) = \lim_{z \rightarrow z_j^*} m(z) \begin{pmatrix} 0 & C_j^* e^{2i\Omega(x, t, z_j^*)} \\ 0 & 0 \end{pmatrix} \quad (2.34b)$$

where $\{C_j\}_{j=1}^N$ are the norming constants defined in terms of the proportionality constants b_j as:

$$C_j = \frac{b_j}{a'(z_j)}. \quad (2.35)$$

Note that the symmetries in Lemma 2 imply that $C_j^* = -e^{2i\theta} C_j$, for all $j = 1, \dots, N$.

4. m has the following asymptotic behavior as $z \rightarrow \infty$ and as $z \rightarrow 0$:

$$m(z) = I_2 + \mathcal{O}(1/z), \quad z \rightarrow \infty, \quad (2.36a)$$

$$m(z) = \frac{q_o}{z} \sigma_2 e^{-i\theta \sigma_3} + \mathcal{O}(1), \quad z \rightarrow 0. \quad (2.36b)$$

Remark 1. In [6] it was established that RHP 1 has a unique solution if and only if $m(z)$ satisfies the following symmetries:

$$m(z) = \sigma_1 m^*(z^*) \sigma_1, \quad m(1/z) = z m(z) \sigma_1. \quad (2.37)$$

In the following lemma, we state the analogous result in our case, to account for the fact that we are using a slightly different normalization for the Jost eigenfunctions as $x \rightarrow \pm\infty$, and also because we consider an IC with arbitrary amplitude q_o and asymptotic phase difference $\theta_+ - \theta_- \equiv 2\theta$, whereas in [6] $q_o = 1$ and $\theta = \pi$. While the generalization to arbitrary $q_o \neq 1$ is not essential, since the amplitude can always be rescaled out, being able to include an arbitrary asymptotic phase difference can be relevant for certain applications.

Lemma 3. If a solution m to RHP 1 exists, then it is unique if and only if it satisfies the symmetries

$$m(z) = \sigma_1 m^*(z^*) \sigma_1, \quad m(q_o^2/z) = \frac{z}{q_o} m(z) \sigma_2 e^{-i\theta \sigma_3}. \quad (2.38)$$

Additionally, for such a solution $\det m(z) = 1 - q_o^2 z^{-2}$.

Proof. The proof of this lemma follows the proof of Lemma 5.3 in [6], after re-adjusting the normalization and the symmetries appropriately. \square

Below, we address the behavior of $m_{\pm}(z)$ at $z = \pm q_o$ for future reference.

Proposition 1. *For the IC (1.3), the solution of RHP 1 is such that $m_{+,1}(z)$ and $m_{-,2}(z)$ have zeros at $z = \pm q_o$ of at least first order, where the superscript $j = 1, 2$ denotes the corresponding column of the matrices $m_{\pm}(z)$.*

Proof. Let m be the solution of RHP 1. Evaluating the jump condition of m at $z = \pm q_o$ we get

$$m_+(x, t, -q_o) = m_-(x, t, -q_o) \begin{pmatrix} 0 & ie^{i\theta} \\ ie^{-i\theta} & 1 \end{pmatrix}, \quad m_+(x, t, q_o) = m_-(x, t, q_o) \begin{pmatrix} 0 & -ie^{i\theta} \\ -ie^{-i\theta} & 1 \end{pmatrix}$$

because $\rho(\pm 1) = \mp ie^{-i\theta}$ (cf. (2.31)). The first column of the last equation gives

$$m_{+,1}(x, t, -q_o) = ie^{-i\theta} m_{-,2}(x, t, -q_o), \quad m_{+,1}(x, t, q_o) = -ie^{-i\theta} m_{-,2}(x, t, q_o). \quad (2.39)$$

Moreover, evaluating the second symmetry relation in (2.38) at $z = \pm q_o$ yields

$$m_{+,1}(x, t, -q_o) = -ie^{-i\theta} m_{-,2}(x, t, -q_o), \quad m_{+,1}(x, t, q_o) = ie^{-i\theta} m_{-,2}(x, t, q_o), \quad (2.40)$$

which together with Eq. (2.39) gives

$$m_{+,1}(x, t, -q_o) = m_{-,2}(x, t, -q_o) = 0, \quad m_{+,1}(x, t, q_o) = m_{-,2}(x, t, q_o) = 0. \quad (2.41)$$

The asymptotic behavior of the scattering data and the analyticity of the modified eigenfunctions at $z = \pm q_o$ forces the above zeros to be of at least first order. \square

Using the asymptotic property of $M_{\pm}(z)$ at infinity and definition (2.32), one then reconstructs the potential via the following relation

$$q(x, t) = \lim_{\substack{z \rightarrow \infty \\ z \in \mathbb{C}^+}} (iz m_{1,2}(x, t, z)) \quad (2.42)$$

where the subscript denotes the 1, 2 entry of the matrix function m .

Our aim is to solve RHP 1 numerically and use relation (2.42) to recover $q(x, t)$ at arbitrary values of $x \in \mathbb{R}$, $t > 0$. However, Eq. (2.36b) shows that m has a singularity at $z = 0$, which is numerically challenging. In the next section we show how the singularity can be removed by an appropriate transformation of the RHP.

3. RHP analysis and contour deformation

This section focuses on two key topics: the development of an appropriate transformation to remove the singularity of the function m in RHP 1 at $z = 0$, and the deformation of contours according to the principles of nonlinear steepest descent method. The goal of the contour deformations is ultimately to convert the oscillatory RHP in Eq. (2.33) for $z \in \mathbb{R}$ into RHPs with jump matrices that are exponentially decaying for $t \rightarrow \infty$. This is the natural approach when one is interested in estimating the long-time asymptotic behavior of the RHP solution and of the corresponding potential $q(x, t)$, but it is also crucial for the numerical solution of an RHP at finite (x, t) .

3.1. Removing the singularity at $z = 0$

Note that the jump matrix $G_m(x, t, z)$ in RHP 1 is well-defined at $z = 0$, and in fact $G_m(x, t, 0) = I_2$. This suggests that we can consider a function \tilde{m} which satisfies the same RHP as m but is non-singular at $z = 0$. Specifically, \tilde{m} satisfies the following RHP.

RHP 2 (RHP for \tilde{m} with solitons). *Find a 2×2 matrix-valued function \tilde{m} such that:*

1. \tilde{m} is sectionally analytic in $\mathbb{C} \setminus \mathbb{R}$

2. The non-tangential limits $\tilde{m}_\pm(x, t, z) = \lim_{\substack{\zeta \rightarrow z \\ \zeta \in \mathbb{C}^\pm}} \tilde{m}_\pm(x, t, \zeta)$ exist for any $z \in \mathbb{R}$ and satisfy the jump relation across the real axis

$$\tilde{m}_+(z) = \tilde{m}_-(z) G_m(x, t, z), \quad G_m(x, t, z) = \begin{pmatrix} 1 - |\rho(z)|^2 & -\rho^*(z) e^{2i\Omega(x, t, z)} \\ \rho(z) e^{-2i\Omega(x, t, z)} & 1 \end{pmatrix} \quad (3.1)$$

3. \tilde{m} has poles at $\{z_j\}_{j=1}^N$ in \mathbb{C}^+ and $\{z_j^*\}_{j=1}^N$ in \mathbb{C}^- satisfying the same residue conditions (2.34) as m
 4. $\tilde{m}(z) = I_2 + \mathcal{O}(1/z)$, $z \rightarrow \infty$
 5. The non-tangential limits of $\tilde{m}(z)$ as $z \rightarrow 0$ from \mathbb{C}^\pm are equal, and

$$\tilde{m}(x, t, 0) := \lim_{\substack{\zeta \rightarrow 0 \\ \zeta \in \mathbb{C}^\pm}} \tilde{m}_\pm(x, t, \zeta).$$

Lemma 4. If a solution \tilde{m} of RHP 2 exists, then it is unique. Additionally, such a solution satisfies the symmetry relations

$$\tilde{m}(z) = \sigma_1 \tilde{m}^*(z^*) \sigma_1, \quad \tilde{m}(z) = \frac{1}{q_o} \sigma_2 \tilde{m}^{-1}(0) \tilde{m}(q_o^2/z) \sigma_2 e^{-i\theta \sigma_3} \quad (3.2)$$

and it is such that $\det \tilde{m}(z) = 1$ for all $z \in \mathbb{C}$.

Proof. First, we show that $\det \tilde{m}(z) = 1$ for all $z \in \mathbb{C}$. Eq. (3.1) implies that

$$\det \tilde{m}_+(z) = \det \tilde{m}_-(z) \det G_m(x, t, z) \equiv \det \tilde{m}_-(z), \quad z \in \mathbb{R} \quad (3.3)$$

which shows that $\det \tilde{m}$ has no jump across the real axis. Moreover, it is easy to check directly from the residue conditions of the function $\tilde{m}(z)$ at z_j that:

$$\begin{aligned} \text{Res}_{z=z_j} \det \tilde{m}(z) &= \lim_{z \rightarrow z_j} \det \tilde{m}(z) (z - z_j) \\ &= \lim_{z \rightarrow z_j} (\tilde{m}_{11}(z) \tilde{m}_{22}(z) - \tilde{m}_{12}(z) \tilde{m}_{21}(z)) (z - z_j) \\ &= \lim_{z \rightarrow z_j} (\tilde{m}_{11}(z) (z - z_j)) \tilde{m}_{22}(z_j) - \lim_{z \rightarrow z_j} (\tilde{m}_{21}(z) (z - z_j)) \tilde{m}_{12}(z_j) \\ &= C_j e^{-2i\Omega(x, t, z_j)} (\tilde{m}_{12}(z_j) \tilde{m}_{22}(z_j) - \tilde{m}_{22}(z_j) \tilde{m}_{12}(z_j)) = 0 \end{aligned}$$

and similarly for z_j^* , which implies that $\det \tilde{m}$ has removable singularities at each $z_j \in \mathbb{C}^+$ and $z_j^* \in \mathbb{C}^-$. Finally, from the large- z asymptotics of \tilde{m} it is immediate that $\det \tilde{m}(z) = 1 + \mathcal{O}(1/z)$, $z \rightarrow \infty$. Therefore, $\det \tilde{m}$ is a bounded, entire function with the given asymptotic behavior. By Liouville's theorem, it follows that $\det \tilde{m}(z) = 1$ for all $z \in \mathbb{C}$.

Uniqueness of solution follows from applying Liouville's theorem to the matrix function $\tilde{m}_1 \tilde{m}_2^{-1}$ where \tilde{m}_1 and \tilde{m}_2 are any two solutions of RHP 2. Eq. (3.1) yields

$$\tilde{m}_{1+}(z) \tilde{m}_{2+}^{-1}(z) = \tilde{m}_{1-}(z) G_m(x, t, z) G_m^{-1}(x, t, z) \tilde{m}_{2-}^{-1}(z) \equiv \tilde{m}_{1-}(z) \tilde{m}_{2-}^{-1}(z) \quad (3.4)$$

which shows that $\tilde{m}_1 \tilde{m}_2^{-1}$ is analytic across the real axis. Furthermore, since \tilde{m}_1 and \tilde{m}_2 satisfy the same residue conditions at z_j and z_j^* , and given that they both have determinant equal one, then we can show that $\tilde{m}_1 \tilde{m}_2^{-1}$ is regular at each $z_j \in \mathbb{C}^+$ and $z_j^* \in \mathbb{C}^-$. Additionally, $\tilde{m}_1 \tilde{m}_2^{-1}$ is non-singular at $z = 0$ because each of the functions \tilde{m}_1 and \tilde{m}_2 is, and $\det \tilde{m}_2(z) = 1$ for all $z \in \mathbb{R}$ excludes additional singularities of $\tilde{m}_2^{-1}(z)$. Finally, $\tilde{m}_1(z) \tilde{m}_2^{-1}(z) = I_2 + \mathcal{O}(1/z)$, as $z \rightarrow \infty$. These imply that $\tilde{m}_1(z) \tilde{m}_2^{-1}(z) = I_2$, for any $z \in \mathbb{C}$, i.e., $\tilde{m}_1(z) = \tilde{m}_2(z)$, for any z .

Finally, we prove the symmetry relations (3.2). Let \tilde{m} be a solution of RHP 2, and let us introduce the matrix functions

$$f_1(z) = \sigma_1 \tilde{m}^*(z^*) \sigma_1, \quad f_2(z) = \frac{1}{q_o} \sigma_2 \tilde{m}^{-1}(0) \tilde{m}(q_o^2/z) \sigma_2 e^{-i\theta\sigma_3} \quad (3.5)$$

which are sectionally analytic in \mathbb{R} because \tilde{m} is. Moreover, we have

$$\begin{aligned} f_{1+}(z) &= \lim_{\substack{\zeta \rightarrow z \\ \zeta \in \mathbb{C}^+}} f_1(\zeta) = \lim_{\substack{\zeta \rightarrow z \\ \zeta \in \mathbb{C}^+}} \sigma_1 \tilde{m}^*(\zeta^*) \sigma_1 = \lim_{\substack{\zeta^* \rightarrow z \\ \zeta^* \in \mathbb{C}^-}} \sigma_1 \tilde{m}^*(\zeta^*) \sigma_1 \\ &= \sigma_1 \tilde{m}_-^*(z) \sigma_1 = \sigma_1 \tilde{m}_+^*(z) \left(G_m^{-1}(x, t, z) \right)^* \sigma_1 = \sigma_1 \tilde{m}_+^*(z) \sigma_1 G_m(x, t, z) \\ &= \lim_{\substack{\zeta \rightarrow z \\ \zeta \in \mathbb{C}^+}} [\sigma_1 \tilde{m}^*(\zeta) \sigma_1] G_m(x, t, z) = \lim_{\substack{\zeta^* \rightarrow z \\ \zeta^* \in \mathbb{C}^-}} [\sigma_1 \tilde{m}^*(\zeta) \sigma_1] G_m(x, t, z) \\ &= \sigma_1 \tilde{m}_-^*(z^*) \sigma_1 G_m(x, t, z) = f_{1-}(z) G_m(x, t, z) \end{aligned}$$

and it is straightforward to see that $f_1(z)$ has trivial asymptotics as $z \rightarrow \infty$, is non-singular at $z = 0$ and satisfies the same residue conditions as $\tilde{m}(z)$. Therefore, by uniqueness of solution, it follows that

$$\tilde{m}(z) = \sigma_1 \tilde{m}^*(z^*) \sigma_1. \quad (3.6)$$

Similar arguments apply to the function $f_2(z)$. \square

We define now the function

$$E(z) = I_2 + \frac{\sigma_2 q_o e^{-i\theta\sigma_3}}{z} \tilde{m}^{-1}(0) \quad (3.7)$$

and we let

$$m(z) = E(z) \tilde{m}(z). \quad (3.8)$$

It is easy to check that if $\tilde{m}(z)$ solves RHP 2, then $m(z)$ defined as in (3.8) is the (unique) solution of RHP 1. Therefore, our approach will be to solve the RHP for $\tilde{m}(x, t, z)$ numerically, and then recover $m(x, t, z)$ via relation (3.8).

3.2. Analysis of the phase function

Recall that our aim is to solve RHP 2 numerically, use it to obtain the solution of RHP 1 via (3.8), and from it compute the potential $q(x, t)$. As shown in [6, 37], the long-time asymptotic analysis identifies three regions in the space-time domain of x and t , depending on the value of the parameter $\xi = x/2t$, with different characteristics: the solitonic region when $|\xi| < q_o$, the solitonless region when $|\xi| > q_o$, and the collisionless shock region when $|\xi| = q_o$. While the analysis in [6, 37] is carried out for the specific case of $q_o = 1$, the results can be generalized to any arbitrary value of q_o . Therefore, we express the jump matrix G_m in (3.1) in terms of ξ as follows

$$G_m(\xi, z) = \begin{pmatrix} 1 - |\rho(z)|^2 & -\rho^*(z) e^{-2t i\Theta(\xi, z)} \\ \rho(z) e^{2t i\Theta(\xi, z)} & 1 \end{pmatrix}, \quad \Theta(\xi, z) = 2(\lambda(z)\xi + k(z)\lambda(z)). \quad (3.9)$$

Note that G_m involves the exponentials $e^{\pm 2t i\Theta(\xi, z)}$ which are oscillatory for $z \in \mathbb{R}$ where the jump of the RHPs is defined. Thus, solving RHP 2 numerically involves implementing contour deformations away from the real axis following the principles of nonlinear steepest descent, similar to those used for estimating the long-time asymptotics (see [9], [8] and [13] for more details). We want to emphasize that the deformations are valid for arbitrary t , and they have the advantage that, for large t , the exponential

decay off the real axis makes the numerical scheme more efficient, by reducing the number of terms that need to be computed. Therefore, we implement the deformations based on the sign chart of $\text{Re}(i\Theta)$ to achieve exponential decay for large t of all the jumps off the real axis.

First, we compute the stationary phase points of the function Θ . We have:

$$\begin{aligned}\Theta'(z) &= \xi \left(1 + q_o^2 z^{-2}\right) + \left(z + q_o^4 z^{-3}\right) \\ &= z^{-1} \left(\xi(z + q_o^2 z^{-1}) + (z + q_o^2 z^{-1})^2 - 2q_o^2\right) \\ &\equiv z^{-1} l(s),\end{aligned}\tag{3.10}$$

where

$$l(s) = s^2 + \xi s - 2q_o^2, \quad s = z + q_o^2 z^{-1},\tag{3.11}$$

and also

$$\Theta''(z) = -z^{-2} l(s) + z^{-1} l'(s) s'(z) \equiv -z^{-2} l(s) + z^{-1} \left(1 - \frac{q_o^2}{z^2}\right) l'(s).\tag{3.12}$$

Simple analysis shows that real zeros of $\Theta'(z)$ exist if and only if $|\xi| \geq q_o$. In particular, we find that the (real) zeros of Θ' , when $|\xi| \geq q_o$, are given by:

$$z_k(\xi) = \frac{1}{2} \left| v(\xi) + (-1)^k \sqrt{v^2(\xi) - 4q_o^2} \right|, \quad k = 1, 2, \quad \xi \leq -q_o,\tag{3.13a}$$

$$\hat{z}_k(\xi) = -\frac{1}{2} \left| v(\xi) + (-1)^k \sqrt{v^2(\xi) - 4q_o^2} \right|, \quad k = 1, 2, \quad \xi \geq q_o,\tag{3.13b}$$

$$v(\xi) = \frac{1}{2} \left(|\xi| + \sqrt{8q_o^2 + \xi^2} \right).\tag{3.13c}$$

It is easy to check that

$$0 < z_1(\xi) < 1 < z_2(\xi), \quad \xi < -q_o,\tag{3.14a}$$

$$\hat{z}_2(\xi) < -1 < \hat{z}_1(\xi) < 0, \quad \xi > q_o.\tag{3.14b}$$

Furthermore, when $\xi = \pm q_o$ the zeros coincide and collapse to the same value $z_k(-q_o) = q_o$ and $\hat{z}_k(q_o) = -q_o$, for $k = 1, 2$. Based on these observations, we can summarize the following:

- There is no stationary phase point on \mathbb{R} when $|\xi| < q_o$.
- There is one stationary phase point on \mathbb{R} when $|\xi| = q_o$.
- There are two stationary phase points on \mathbb{R} when $|\xi| > q_o$.

Finally, a direct calculation yields

$$\text{Re}(i\Theta(\xi, z)) = -\xi \text{Im} z \left(1 + \frac{q_o^2}{|z|^2}\right) - \text{Re} z \text{Im} z \left(1 + \frac{q_o^4}{|z|^4}\right).\tag{3.15}$$

Fig. 2 shows the sign chart of $\text{Re}(i\Theta)$ in the three regions for $q_o = 1$, along with the location of the stationary phase points in each region. The same figures can be obtained for arbitrary q_o but the range of x -values must be scaled appropriately to account for the location of the stationary phase points.

Remark 2. *It is clear from Fig. 2 that the required contour deformations will be different in the three regions, and they also depend on whether solitons are present or not. For the remainder of this paper, we focus on a box-type IC that does not support solitons, and we solve the associated RHP numerically*

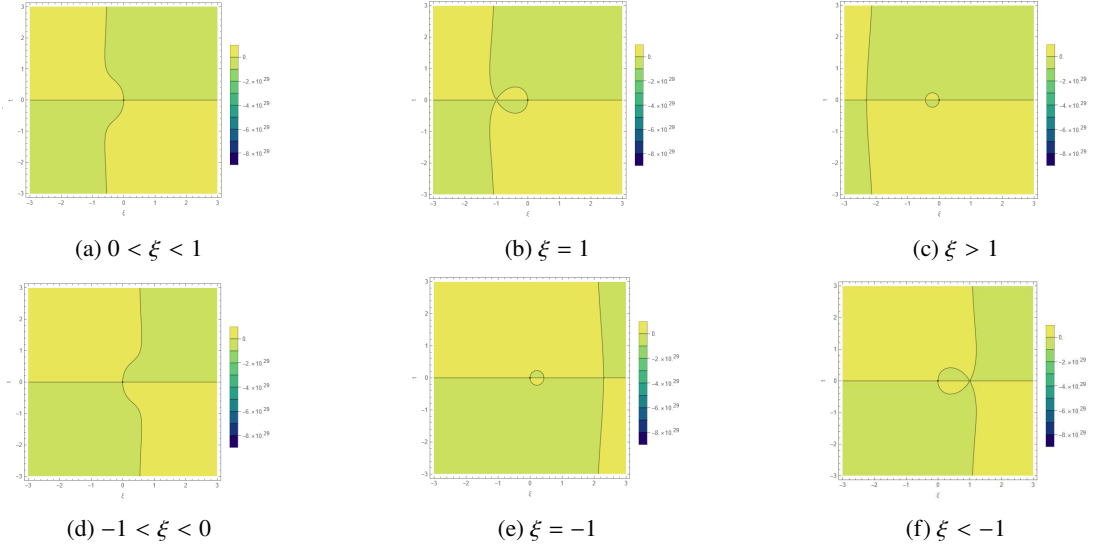


Figure 2: The sign chart of $\text{Re}(i\Theta)$, when $|\xi| < 1$, $|\xi| > 1$ and $|\xi| = 1$ for the specific case $q_o = 1$. The yellow region corresponds to $\text{Re}(i\Theta) > 0$, and the green region corresponds to $\text{Re}(i\Theta) < 0$.

in the solitonic and solitonless regions. The case of solitons is beyond the scope of this study, and will be addressed in a future work. Additionally, the detailed study of the deformations in the collisionless shock region remains an open problem also as far as the long-time asymptotics is concerned. As we will show in Sec 4, however, the numerical solution of the RHP in each of the regions $|\xi| < q_o$ and $|\xi| > q_o$ actually extends well beyond the boundaries of the domain, and the potentials reconstructed in each region show excellent agreement with each other, at least for bounded times. This seems to indicate that for the purpose of the numerical IST a separate study of the collisionless shock region, though desirable, is not required to compute solution profiles.

In the following, we are going to assume that the IC is of box-type, and specifically of the form (1.3). As shown in [5], if the asymptotic phase difference $\theta = 0$ and $0 < h < q_o$, the scattering problem always has at least one discrete eigenvalue. On the other hand, if $\theta = 0$ and $h > q_o$, any choice of the box width L , and any $\alpha \in [0, \pi]$ satisfying:

$$0 \leq \alpha < \arccos(q_o/h) \quad (3.16)$$

yields an IC for which no discrete eigenvalue is present. Conversely, if we assume $\alpha = 0$, for any choice of L and $h > q_o$, any sufficiently small asymptotic phase difference θ , satisfying the condition

$$\sin \theta < \left(1 - \frac{q_o}{h}\right) \tanh \left(2q_o L \sqrt{\frac{h^2}{q_o^2} - 1}\right) \quad (3.17)$$

(cf. Eq. (45) in [5]) also produces ICs with no discrete eigenvalues.

For definiteness, we consider Eq. (1.1) with NZBCs (1.2), IC (1.3), and the values

$$L = 1, \quad q_o = 1, \quad \theta = 0, \quad \alpha = 0, \quad h = 1.5. \quad (3.18)$$

For these box parameter values, the expressions (2.25) for the scattering coefficients and the reflection coefficient simplify to

$$a(z) = e^{2i\lambda(z)} \left(\cos(2\mu(z)) + i \frac{h - k^2(z)}{\lambda(z)\mu(z)} \sin(2\mu(z)) \right), \quad (3.19a)$$

$$b(z) = \frac{k(z)(h-1)}{\lambda(z)\mu(z)} \sin(2\mu(z)), \quad (3.19b)$$

$$\rho(z) = e^{-2i\lambda(z)} \left(\frac{ik(z)(h-1)}{k^2(z) - h + i\lambda(z)\mu(z) \cot(2\mu(z))} \right), \quad (3.19c)$$

with:

$$k(z) = \frac{1}{2}(z + 1/z), \quad \lambda(z) = \frac{1}{2}(z - 1/z), \quad \mu(z) = \sqrt{k(z)^2 - h^2}. \quad (3.20)$$

The box parameters (3.18) are chosen so that $a(z)$ has no zeros in \mathbb{C}^+ (and $a^*(z^*)$ has no zeros in \mathbb{C}^-), indicating no solitons are present. Other choices of parameters which yield a purely radiative (i.e., solitonless) solution, e.g., satisfying (3.16) or (3.17), will also be considered for illustrative purposes.

It is worth mentioning that since we are currently restricting ourselves to the solitonless case, $\tilde{q}(x) + H^{1,1}(\mathbb{R})$ provides an appropriate space for the ICs. Although our box-type ICs do not lie in this space, due to their piecewise-smooth, compactly supported (in relation to the background) nature, the scattering theory can nonetheless be implemented, analytically and numerically, without a hitch, giving an appropriately analytic reflection coefficient.

As pointed out in Sec 2, the scattering data generically have simple poles at $z = \pm q_o$ unless the columns of M_{\pm} are linearly dependent at $z = q_o$ or $z = -q_o$ or both, in which case $\alpha_{\pm} = 0$. However, in this case it is straightforward to verify that $\alpha_{\pm} \neq 0$. Moreover, the reflection coefficient can be analytically continued off the real z -axis, and it is in fact analytic in the entire complex plane. In this case, RHP 2 simplifies into the following one.

RHP 3 (RHP for \tilde{m} without solitons). *Find a 2×2 matrix-valued function $\tilde{m}(z)$ such that:*

1. $\tilde{m}(z)$ is sectionally analytic in $\mathbb{C} \setminus \mathbb{R}$
2. The non-tangential limits $\tilde{m}_{\pm}(z) = \lim_{\zeta \rightarrow z} \tilde{m}_{\pm}(\zeta)$ exist for any $z \in \mathbb{R}$ and satisfy the jump relation across the real axis

$$\tilde{m}_+(z) = \tilde{m}_-(z)G_m(\xi, z), \quad G_m(\xi, z) = \begin{pmatrix} 1 - |\rho(z)|^2 & -\rho^*(z)e^{-2t i\Theta(\xi, z)} \\ \rho(z)e^{2t i\Theta(\xi, z)} & 1 \end{pmatrix} \quad (3.21)$$

3. $\tilde{m}(z) = I_2 + \mathcal{O}(1/z)$, $z \rightarrow \infty$
4. The non-tangential limits of $\tilde{m}(z)$ as $z \rightarrow 0$ from \mathbb{C}^{\pm} are equal, namely $\tilde{m}_+(0) = \tilde{m}_-(0) =: \tilde{m}(0)$.

Note that Lemma 4 also applies to RHP 3. In the following sections, we provide the necessary deformations that lead to a numerical method that is accurate for an arbitrary (x, t) in both the solitonic and the solitonless regions.

3.3. Jump matrix factorizations

Direct calculations show that G_m has the following two factorizations:

$$G_m(\xi, z) = M(\xi, z)P(\xi, z) \equiv L(\xi, z)D(z)U(\xi, z), \quad (3.22)$$

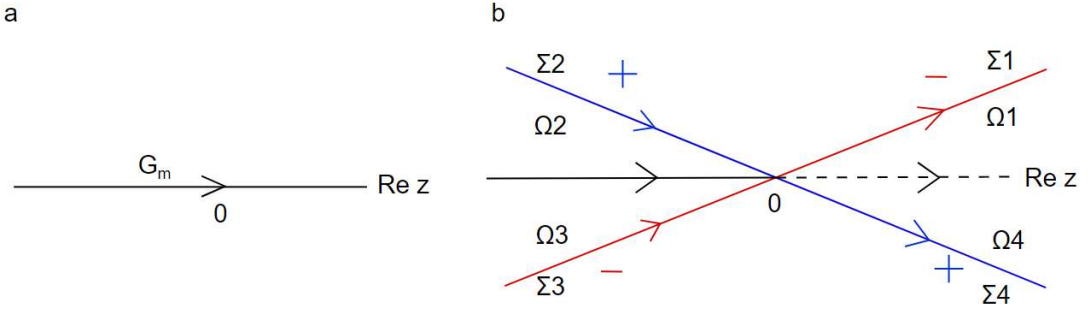


Figure 3: Panel a: the initial jump for the function m . Panel b: the new jump contours after we open lenses in the solitonic region, and the sign of $\text{Re}(i\Theta)$ when $-1 < \xi < 1$. + indicates that $\text{Re}(i\Theta) > 0$ in the corresponding regions, and - stands for $\text{Re}(i\Theta) < 0$.

where

$$M(\xi, z) = \begin{pmatrix} 1 & -\rho^*(z)e^{-2t i\Theta(\xi, z)} \\ 0 & 1 \end{pmatrix}, \quad P(\xi, z) = \begin{pmatrix} 1 & 0 \\ \rho(z)e^{2t i\Theta(\xi, z)} & 1 \end{pmatrix}, \quad (3.23a)$$

$$L(\xi, z) = \begin{pmatrix} 1 & 0 \\ \frac{\rho(z)}{1-|\rho(z)|^2} e^{2t i\Theta(\xi, z)} & 1 \end{pmatrix}, \quad U(\xi, z) = \begin{pmatrix} 1 - \frac{\rho^*(z)}{1-|\rho(z)|^2} e^{-2t i\Theta(\xi, z)} & \\ 0 & 1 \end{pmatrix}, \quad (3.23b)$$

$$D(z) = \begin{pmatrix} 1 - |\rho(z)|^2 & 0 \\ 0 & \frac{1}{1-|\rho(z)|^2} \end{pmatrix}. \quad (3.23c)$$

Note that each of the matrices P, M, L , and U involves only one of the exponents $e^{\pm 2t i\Theta(\xi, z)}$, and therefore depending on the sign of $\text{Re}(i\Theta)$, we use the appropriate factorizations of G_m in the appropriate regions off the real axis. Next, we present the deformations in the solitonic and solitonless region, separately.

3.4. Solitonic region

In this subsection, we provide the required contour deformations in the solitonic region, corresponding to $\xi \in (-1, 1)$. First, we choose a sufficiently small positive angle ϕ to ensure the deformed contours remain inside regions with the same sign in the sign chart and open lenses around $z = 0$. While $\phi = \pi/4$ is the optimal choice for the direction of the fastest decay in the nonlinear steepest descent method, the primary requirement is simply to select a small positive angle ϕ that maintains the consistency of the sign in the sign chart of $\text{Re}(i\Theta)$. Four new regions are therefore created, which we denote by Ω_k , $k = 1, \dots, 4$, given by

$$\Omega_1 = \{z : \arg z \in (0, \phi)\}, \quad \Omega_2 = \{z : \arg z \in (\pi - \phi, \pi)\}, \quad (3.24a)$$

$$\Omega_3 = \{z : \arg z \in (-\pi, -\pi + \phi)\}, \quad \Omega_4 = \{z : \arg z \in (-\phi, 0)\}. \quad (3.24b)$$

Finally, denote by

$$\Sigma_1 = e^{i\phi} \mathbb{R}_+, \quad \Sigma_2 = e^{i(\pi-\phi)} \mathbb{R}_+, \quad \Sigma_3 = e^{-i(\pi-\phi)} \mathbb{R}_+, \quad \Sigma_4 = e^{-i\phi} \mathbb{R}_+, \quad (3.25a)$$

the left-to-right oriented boundaries of $\Omega = \bigcup_{k=1}^4 \Omega_k$, see Fig. 3. Panels (a) and (d) in Fig. 2 suggest to use the LDU-factorization in the regions $\Omega_2 \cup \Omega_3$, and the PM-factorization in the regions $\Omega_1 \cup \Omega_4$.

Next, we define the function $m_{1,d}$:

$$m_{1,d}(z) = \begin{cases} \tilde{m}(z)P^{-1}(\xi, z), & z \in \Omega_1 \\ \tilde{m}(z)U^{-1}(\xi, z), & z \in \Omega_2 \\ \tilde{m}(z)L(\xi, z), & z \in \Omega_3 \\ \tilde{m}(z)M(\xi, z), & z \in \Omega_4 \\ \tilde{m}(z), & \text{elsewhere} \end{cases} \quad (3.26)$$

which satisfies the following RHP.

RHP 4 (RHP for $m_{1,d}$). Find a 2×2 matrix-valued function $m_{1,d}$ such that:

1. $m_{1,d}$ is analytic in $\mathbb{C} \setminus \Sigma$, where $\Sigma = (-\infty, 0) \cup \bigcup_{j=1}^4 \Sigma_j$
2. $m_{1,d}$ satisfies the jump relation across Σ

$$m_{1,d+}(z) = m_{1,d-}(z)G_{m_{1,d}}(\xi, z), \quad z \in \Sigma \quad (3.27a)$$

with $G_{m_{1,d}}$ given by

$$G_{m_{1,d}}(\xi, z) = \begin{cases} P(\xi, z), & z \in \Sigma_1 \\ U(\xi, z), & z \in \Sigma_2 \\ L(\xi, z), & z \in \Sigma_3 \\ M(\xi, z), & z \in \Sigma_4 \\ D(z), & z \in (-\infty, 0) \end{cases} \quad (3.27b)$$

Here, $+/-$ are the limiting values of the function $m_{1,d}$ as z approaches the oriented contours of non-analyticity from the left and right, respectively.

3. $m_{1,d}(z) = I_2 + \mathcal{O}(1/z)$, $z \rightarrow \infty$
4. The non-tangential limits of $m_{1,d}(z)$ as $z \rightarrow 0$ from \mathbb{C}^\pm exist, and $m_{1,d+}(0) = m_{1,d-}(0) =: m_{1,d}(0)$.

Note that the function $m_{1,d}$ depends both on ξ and z . For the sake of brevity, we omit the dependence on ξ . The same holds also in the subsequent transformations, including those in the solitonless region.

Remark 3. Notice that for large t , the jumps across Σ_j , for $j = 1, \dots, 4$ are exponentially close to the identity matrix, as the exponents $e^{\pm 2t i \Theta(\xi, z)}$ decay rapidly. This leads to increased efficiency in the numerical scheme for large t , since fewer terms need to be computed. However, this does not happen with the jump matrix D across $(-\infty, 0)$.

To remove the jump across \mathbb{R}^- , we introduce the function

$$m_{2,d}(z) = m_{1,d}(z)\Delta^{-1}(z) \quad (3.28)$$

with Δ given explicitly by

$$\Delta(z) = \text{diag}\left(\delta(z), 1/\delta(z)\right), \quad \delta(z) = \exp\left[\frac{1}{2\pi i} \int_{-\infty}^0 \frac{\log(1 - |\rho(s)|^2)}{s - z} ds\right], \quad (3.29)$$

where $\delta(z)$ satisfies the following scalar RHP.

RHP 5 (RHP for δ). Find a scalar function $\delta(z)$ such that:

1. δ is analytic in $\mathbb{C} \setminus (-\infty, 0)$
2. δ satisfies the jump relation

$$\delta_+(z) = \delta_-(z) \left(1 - |\rho(z)|^2\right), \quad z \in (-\infty, 0) \quad (3.30)$$

3. $\delta(z) = 1 + O(1/z)$ as $z \rightarrow \infty$
4. $\delta(z)$ has the following asymptotic behavior as $z \rightarrow -1$:

$$\delta(z)|z+1|^{-1} = O(1), \quad z \rightarrow -1, \quad z \in \mathbb{C}^+ \quad (3.31a)$$

$$\delta(z)|z+1| = O(1), \quad z \rightarrow -1, \quad z \in \mathbb{C}^-. \quad (3.31b)$$

In Sec 4 and in Appendix A, we provide details on the numerical computation and the analytical derivation of the function δ .

In light of RHP 5, the function $m_{2,d}$ in (3.28) satisfies the following RHP.

RHP 6 (RHP for $m_{2,d}$). *Find a 2×2 matrix-valued function $m_{2,d}$ such that:*

1. $m_{2,d}$ is analytic in $\mathbb{C} \setminus \Sigma'$, where $\Sigma' = \bigcup_{j=1}^4 \Sigma_j$
2. $m_{2,d}$ satisfies the jump relation across Σ'

$$m_{2,d+}(z) = m_{2,d-}(z) G_{m_{2,d}}(\xi, z), \quad z \in \Sigma' \quad (3.32a)$$

where the jump matrix is given by

$$G_{m_{2,d}}(\xi, z) = \begin{cases} \Delta(z)P(\xi, z)\Delta^{-1}(z), & z \in \Sigma_1 \\ \Delta(z)U(\xi, z)\Delta^{-1}(z), & z \in \Sigma_2 \\ \Delta(z)L(\xi, z)\Delta^{-1}(z), & z \in \Sigma_3 \\ \Delta(z)M(\xi, z)\Delta^{-1}(z), & z \in \Sigma_4 \end{cases} \quad (3.32b)$$

3. $m_{2,d}(z) = I_2 + O(1/z)$, $z \rightarrow \infty$
4. The non-tangential limits of $m_{2,d}(z)$ as $z \rightarrow 0$ from \mathbb{C}^\pm exist, and $m_{2,d+}(0) = m_{2,d-}(0) =: m_{2,d}(0)$.

Remark 4. Note that the jump $D(z)$ of the function $m_{1,d}$ across $(-\infty, 0)$ becomes singular at $z = -1$ since the reflection coefficient is such that $\rho(-1) = i$. Therefore, it is necessary to analyze the behavior of $m_{2,d}(z)$ at $z = -1$, and whether it inherits a singularity from the function $m_{1,d}(z)$. In general, D becomes singular at both $z = \pm 1$. However, within the solitonic region, only the singularity at $z = -1$ is significant, since D is the jump matrix across $(-\infty, 0)$. In contrast, as we will see in Sec 4, in the solitonless region both singularities at $z = -1$ and $z = 1$ play a role.

Proposition 2. *The boundary values of the function $m_{2,d}(z)$ at $z = -1$ are bounded.*

Proof. We recall the definition (3.28) of $m_{2,d}(z)$ where $m_{1,d}(z)$ is given by (3.26). We have:

$$\begin{aligned} m_{2,d-}(-1) &= \lim_{\substack{\zeta \rightarrow -1 \\ \zeta \in \mathbb{C}^-}} m_{1,d}(\zeta) \Delta^{-1}(\zeta) = \lim_{\substack{\zeta \rightarrow -1 \\ \zeta \in \mathbb{C}^-}} \tilde{m}(\zeta) L(\zeta) \Delta^{-1}(\zeta) \\ &= \lim_{\substack{\zeta \rightarrow -1 \\ \zeta \in \mathbb{C}^-}} E^{-1}(\zeta) m(\zeta) L(\zeta) \Delta^{-1}(\zeta) \\ &= \lim_{\substack{\zeta \rightarrow -1 \\ \zeta \in \mathbb{C}^-}} E^{-1}(\zeta) \begin{pmatrix} m_1(\zeta) & m_2(\zeta) \end{pmatrix} \begin{pmatrix} 1 & 0 \\ \frac{\rho(\zeta)}{1-|\rho(\zeta)|^2} e^{2i\theta(\xi, \zeta)} & 1 \end{pmatrix} \text{diag} (1/\delta(\zeta) \ \delta(\zeta)) \end{aligned}$$

$$\begin{aligned}
 &= \lim_{\zeta \rightarrow -1} E^{-1}(\zeta) \begin{pmatrix} m_{-,1}(\zeta) & m_{-,2}(\zeta) \end{pmatrix} \begin{pmatrix} 1 & 0 \\ \frac{\rho(\zeta)}{1-|\rho(\zeta)|^2} e^{2t i\Theta(\xi, \zeta)} & 1 \end{pmatrix} \text{diag} (1/\delta_-(\zeta) \ \delta_-(\zeta)) \\
 &= \lim_{\zeta \rightarrow -1} E^{-1}(\zeta) \left(\frac{1}{\delta_-(\zeta)} m_{-,1}(\zeta) + \frac{1}{\delta_-(\zeta)} \frac{\rho(\zeta) e^{2t i\Theta(\xi, \zeta)}}{1-|\rho(\zeta)|^2} m_{-,2}(\zeta) \ \delta_-(\zeta) m_{-,2}(\zeta) \right). \quad (3.33)
 \end{aligned}$$

Notice that the quantity $\frac{\rho(\zeta) e^{2t i\Theta(\xi, \zeta)}}{1-|\rho(\zeta)|^2}$ is singular at $\zeta = -1$. However, by applying proposition 1 to the IC (1.3) with parameters (3.18) for $z = \pm 1$, we can conclude that both $m_{+,1}(z)$ and $m_{-,2}(z)$ have zeros at $z = \pm 1$ of at least first order. Together with the behavior of $\delta(z)$ as z approaches -1 from \mathbb{C}^- , this implies that the second matrix function appearing in (3.33) is bounded. Moreover, from Eq. (3.7) it follows that $E^{-1}(-1)$ is a constant matrix

$$E^{-1}(-1) = I_2 - \sigma_2 \tilde{m}^{-1}(0).$$

Similarly, we have:

$$\begin{aligned}
 m_{2,d+}(-1) &= \lim_{\substack{\zeta \rightarrow -1 \\ \zeta \in \mathbb{C}^+}} m_{1,d}(\zeta) \Delta^{-1}(\zeta) = \lim_{\substack{\zeta \rightarrow -1 \\ \zeta \in \mathbb{C}^+}} \tilde{m}(\zeta) U^{-1}(\zeta) \Delta^{-1}(\zeta) \\
 &= \lim_{\substack{\zeta \rightarrow -1 \\ \zeta \in \mathbb{C}^+}} E^{-1}(\zeta) m(\zeta) U^{-1}(\zeta) \Delta^{-1}(\zeta) \\
 &= \lim_{\substack{\zeta \rightarrow -1 \\ \zeta \in \mathbb{C}^+}} E^{-1}(\zeta) \begin{pmatrix} m_1(\zeta) & m_2(\zeta) \end{pmatrix} \begin{pmatrix} 1 & \frac{\rho^*(\zeta)}{1-|\rho(\zeta)|^2} e^{-2t i\Theta(\xi, \zeta)} \\ 0 & 1 \end{pmatrix} \text{diag} (1/\delta(\zeta) \ \delta(\zeta)) \\
 &= \lim_{\zeta \rightarrow -1} E^{-1}(\zeta) \begin{pmatrix} m_{+,1}(\zeta) & m_{+,2}(\zeta) \end{pmatrix} \begin{pmatrix} 1 & \frac{\rho^*(\zeta)}{1-|\rho(\zeta)|^2} e^{-2t i\Theta(\xi, \zeta)} \\ 0 & 1 \end{pmatrix} \text{diag} (1/\delta_+(\zeta) \ \delta_+(\zeta)) \\
 &= \lim_{\zeta \rightarrow -1} E^{-1}(\zeta) \left(\frac{1}{\delta_+(\zeta)} m_{+,1}(\zeta) \ \delta_+(\zeta) m_{+,2}(\zeta) + \frac{\rho^*(\zeta) e^{-2t i\Theta(\xi, \zeta)}}{1-|\rho(\zeta)|^2} \delta_+(\zeta) m_{+,1}(\zeta) \right). \quad (3.34)
 \end{aligned}$$

The quantity $\frac{\rho^*(\zeta) e^{-2t i\Theta(\xi, \zeta)}}{1-|\rho(\zeta)|^2}$ becomes singular at $\zeta = -1$. However, again by using Proposition 1 and the behavior of $\delta(z)$ as z approaches -1 from \mathbb{C}^+ , we can check that the second matrix function appearing in (3.34) is bounded. \square

Using the above deformations one can compute $m_{2,d}(z)$ numerically for any z . However, the potential $q(x, t)$ is reconstructed via (2.42) in terms of the solution of the initial RHP formulated for $m(z)$, and therefore we need to relate (2.42) to $m_{2,d}(z)$. From Eqs. (3.7) and (3.8), we have

$$m(x, t, z) = \left(I_2 + \frac{\sigma_2}{z} \tilde{m}^{-1}(x, t, 0) \right) \tilde{m}(x, t, z) \quad (3.35)$$

which is equivalent to

$$m(x, t, z) = \left(I_2 + \frac{\sigma_2}{z} \Delta^{-1}(0) m_{2,d}^{-1}(x, t, 0) \right) m_{2,d}(x, t, z) \Delta(z), \quad z \in \mathbb{C} \setminus \bigcup_{j=1}^4 \Omega_j \quad (3.36)$$

where we have replaced $\tilde{m}(z) = m_{2,d}(z) \Delta(z)$, for $z \in \mathbb{C} \setminus \Omega_j$, $j = 1, \dots, 4$, according to (3.26) and (3.28). For $z \in \Omega_j$ one can still write the equivalent expression of \tilde{m} in terms of $m_{2,d}$ using the respective definition of $m_{1,d}$ in each region. However, the potential $q(x, t)$ is determined by the behavior of $m(x, t, z)$ as $z \rightarrow \infty$, and $m_{1,d}$ coincides with m for large- z . Thus, Eq. (3.36) is sufficient for this purpose. Using

equations (2.42) and (3.36), one can recover the potential $q(x, t)$ for any (x, t) via the relation

$$q(x, t) = i \left(\left(m_{2,d}^{(-1)}(x, t) \right)_{1,2} + \left(\sigma_2 \Delta^{-1}(0) m_{2,d}^{-1}(x, t, 0) \right)_{1,2} \right) \quad (3.37)$$

where $m_{2,d}^{(-1)}(x, t)$ is the $\mathcal{O}(1/z)$ -order asymptotics of the function $m_{2,d}$ as $z \rightarrow \infty$, and the subscript denotes the $(1, 2)$ entry of the prescribed matrix.

Remark 5. Note that the uniqueness result for RHP 1 presented in [6] (see Remark 1) can be adapted to our context. First, recall that we can express m in terms of $m_{2,d}$ via relation (3.36). To ensure uniqueness of m , it follows that functions $m_{2,d}$ and Δ must satisfy the symmetries

$$\Delta(z) = \sigma_1 \Delta^*(z^*) \sigma_1, \quad \Delta(z^{-1}) = \sigma_2 \Delta(z) \sigma_2 \quad (3.38a)$$

$$m_{2,d}(z) = \sigma_1 m_{2,d}^*(z^*) \sigma_1, \quad m_{2,d}(z^{-1}) = \sigma_2 \Delta^{-1}(0) m_{2,d}^{-1}(0) m_{2,d}(z) \sigma_2. \quad (3.38b)$$

Now, the definition (3.29) for Δ satisfies the first symmetry in (3.38a), but not the second one. To remedy this, one can define $\tilde{\Delta}$ as in [6], namely

$$\tilde{\Delta}(z) = \text{diag} \left(\tilde{\delta}(z), 1/\tilde{\delta}(z) \right), \quad \tilde{\delta}(z) = \delta(z) \exp \left[-\frac{1}{4\pi i} \int_{-\infty}^0 \frac{\log(1 - |\rho(s)|^2)}{s} ds \right] \quad (3.39)$$

and one can check that $\tilde{\Delta}$ in (3.39) satisfies both symmetries. However, in this case, $\tilde{\Delta}$ does not have trivial asymptotics for large- z , since as $z \rightarrow \infty$

$$\tilde{\Delta}(z) = \tilde{\Delta}_\infty + \mathcal{O}(1/z), \quad \tilde{\Delta}_\infty = \text{diag} \left(\tilde{\delta}_\infty, 1/\tilde{\delta}_\infty \right), \quad \tilde{\delta}_\infty = \exp \left[-\frac{1}{4\pi i} \int_{-\infty}^0 \frac{\log(1 - |\rho(s)|^2)}{s} ds \right].$$

Therefore, to ensure that $m_{2,d}$ has trivial large- z asymptotics, we can define

$$m_{2,d}(z) = m_{1,d}(z) \tilde{\Delta}_\infty \tilde{\Delta}^{-1}(z). \quad (3.40)$$

In this case, $m_{2,d}$ satisfies the symmetries

$$m_{2,d}(z) = \sigma_1 m_{2,d}^*(z^*) \sigma_1, \quad m_{2,d}(z^{-1}) = \sigma_2 \tilde{\Delta}_\infty \tilde{\Delta}^{-1}(0) m_{2,d}^{-1}(0) m_{2,d}(z) \sigma_2 \quad (3.41)$$

and m given by the reconstruction formula

$$m(z) = \left(I_2 + \frac{\sigma_2}{z} \tilde{\Delta}_\infty \tilde{\Delta}^{-1}(0) m_{2,d}^{-1}(0) \right) m_{2,d}(z) \tilde{\Delta}(z) \tilde{\Delta}_\infty^{-1} \quad (3.42)$$

satisfies symmetries (2.37), which implies that m is unique. From a numerical point of view, both definitions Δ and $\tilde{\Delta}$ are equally suitable.

In Sec 4 we will discuss how to implement a numerical scheme to compute the solution to RHP 6 in the soliton region numerically by solving the corresponding integral equations for $m_{2,d}$ using the RHPackage [26] and ISTPackage packages [30].

3.5. Solitonless region

In this section, we describe the required contour deformations in the solitonless region in the case $\xi < -1$, see panel (f) in Fig. 2. When $\xi > 1$ (panel (c) in Fig. 2), the sign chart changes, but the

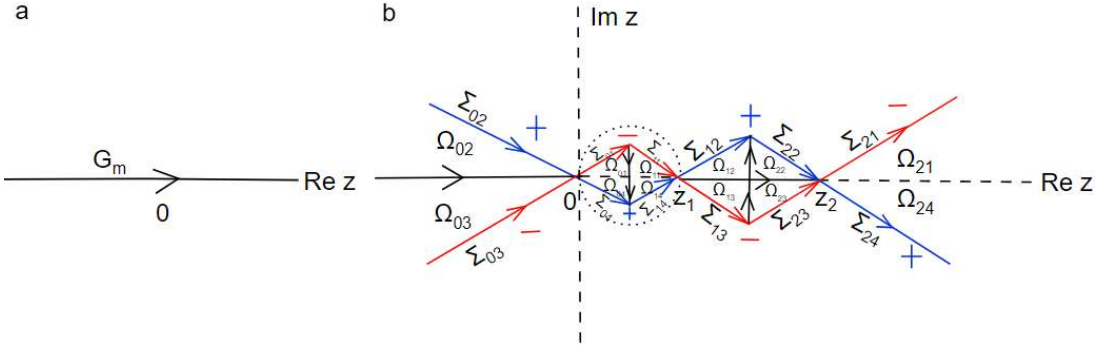


Figure 4: Panel a: the initial jump for the function m . Panel b: the new jump contours after we open lenses in the solitonless region when $\xi < -1$, and the sign of $\text{Re}(i\Theta)$, where $+$ indicates the real part $\text{Re}(i\Theta) > 0$ in the corresponding regions, and $-$ stands for $\text{Re}(i\Theta) < 0$.

approach for the deformations is similar, and we will discuss it briefly at the end of this section. In the solitonless region, unlike the solitonic region, the phase function Θ has two real stationary phase points. Thus, we fix a sufficiently small positive angle ϕ to ensure the deformed contours remain inside regions with the same sign in the sign chart, and open lenses around the origin and the two stationary phase points, z_1 and z_2 . Let us consider the real intervals

$$l_1 \in \left(0, \frac{|z_1|}{2} \sec \phi\right), \quad l_2 \in \left(0, \frac{|z_2 - z_1|}{2} \sec \phi\right) \quad (3.43)$$

and denote the boundaries produced after opening lenses by Σ_{kj} :

$$\Sigma_{01} = e^{i\phi}l_1, \quad \Sigma_{02} = e^{i(\pi-\phi)}\mathbb{R}^+, \quad \Sigma_{11} = z_1 + e^{i(\pi-\phi)}l_1, \quad \Sigma_{12} = z_1 + e^{i\phi}l_2 \quad (3.44a)$$

$$\Sigma_{21} = z_2 + e^{i\phi}\mathbb{R}^+, \quad \Sigma_{22} = z_2 + e^{i(\pi-\phi)}l_2 \quad (3.44b)$$

$$\Sigma_{k4} = \Sigma_{k1}^*, \quad \Sigma_{k3} = \Sigma_{k2}^*, \quad k = 0, 1, 2. \quad (3.44c)$$

We then denote by Ω_{kj} , $k = 0, 1, 2$ and $j = 1, \dots, 4$ the 12 new regions enclosed by the above boundaries, see Fig. 4. Based on panel (f) in Fig. 2, we have

$$\text{Re}(i\Theta(z)) > 0, \quad \text{for } z \in \Omega_{kj}, \quad k = 0, 1, 2, \quad j = 2, 4 \quad (3.45a)$$

$$\text{Re}(i\Theta(z)) < 0, \quad \text{for } z \in \Omega_{kj}, \quad k = 0, 1, 2, \quad j = 1, 3, \quad (3.45b)$$

which suggests to use the LDU factorization for the jump matrix G_m in the regions Ω_{kj} , for $k = 0, 1, 2$ and $j = 2, 3$, and the PM factorization in the regions Ω_{kj} , for $k = 0, 1, 2$ and $j = 1, 4$. Accordingly, we define the function $m_{1,d}$ as follows:

$$m_{1,d}(z) := m_{1,d}(\xi, z) = \begin{cases} \tilde{m}(z)P^{-1}(\xi, z), & z \in \Omega_{01} \cup \Omega_{11} \cup \Omega_{21} \\ \tilde{m}(z)U^{-1}(\xi, z), & z \in \Omega_{02} \cup \Omega_{12} \cup \Omega_{22} \\ \tilde{m}(z)L(\xi, z), & z \in \Omega_{03} \cup \Omega_{13} \cup \Omega_{23} \\ \tilde{m}(z)M(\xi, z), & z \in \Omega_{04} \cup \Omega_{14} \cup \Omega_{24} \\ \tilde{m}(z), & \text{elsewhere} \end{cases} \quad (3.46)$$

which satisfies the following RHP.

RHP 7 (RHP for $m_{1,d}$). Find a 2×2 matrix-valued function $m_{1,d}$ such that:

1. $m_{1,d}$ is analytic in $\mathbb{C} \setminus \Sigma$, where $\Sigma = (z_1, z_2) \cup (-\infty, 0) \cup \bigcup_{k=0}^2 \bigcup_{j=1}^4 \Sigma_{kj}$
2. $m_{1,d}$ satisfies the jump relation across Σ

$$m_{1,d+}(z) = m_{1,d-}(z)G_{m_{1,d}}(\xi, z), \quad z \in \Sigma \quad (3.47a)$$

with $G_{m_{1,d}}$ given by

$$G_{m_{1,d}}(\xi, z) = \begin{cases} P(\xi, z), & z \in \Sigma_{01} \cup \Sigma_{11} \cup \Sigma_{21} \\ U(\xi, z), & z \in \Sigma_{02} \cup \Sigma_{12} \cup \Sigma_{22} \\ L(\xi, z), & z \in \Sigma_{03} \cup \Sigma_{13} \cup \Sigma_{23} \\ M(\xi, z), & z \in \Sigma_{04} \cup \Sigma_{14} \cup \Sigma_{24} \\ D(z), & z \in (-\infty, 0) \cup (z_1, z_2) \end{cases} \quad (3.47b)$$

$$3. \quad m_{1,d}(z) = I_2 + \mathcal{O}(1/z), \quad z \rightarrow \infty$$

4. The non-tangential limits of $m_{1,d}(z)$ as $z \rightarrow 0$ from \mathbb{C}^\pm exist, and $m_{1,d+}(0) = m_{1,d-}(0) =: m_{1,d}(0)$.

Like in the solitonic region, we need to introduce an appropriate function $\hat{\Delta}$ to remove the jump matrix $D(z)$ across $(-\infty, 0) \cup (z_1, z_2)$. Note that in general, $\hat{\Delta}$ is singular at the stationary phase points. To properly handle the singularities, we introduce circles around both z_1 and z_2 , see Fig. 5. This introduces new regions, denoted by ω_j, ω'_j , for $j = 1, \dots, 6$, see Figs. 5 and 6.

We define the function $m_{2,d}$ as follows:

$$m_{2,d}(z) := m_{2,d}(\xi, z) = \begin{cases} m_{1,d}(z)U^{-1}(\xi, z)\hat{\Delta}(z), & z \in \omega_1 \cup \omega'_1 \\ m_{1,d}(z)P(\xi, z)U^{-1}(\xi, z)\hat{\Delta}(z), & z \in \omega_2 \cup \omega_3 \cup \omega'_5 \cup \omega'_6 \\ m_{1,d}(z)M(\xi, z)P(\xi, z)U^{-1}(\xi, z)\hat{\Delta}(z), & z \in \omega_4 \cup \omega'_4 \\ m_{1,d}(z)D(z)\hat{\Delta}(z), & z \in \omega_5 \cup \omega'_3 \\ m_{1,d}(z)\hat{\Delta}(z), & z \in \omega_6 \cup \omega'_2 \\ m_{1,d}(z), & \text{elsewhere} \end{cases} \quad (3.48)$$

which satisfies the following RHP.

RHP 8 (RHP for $m_{2,d}$). Find a 2×2 matrix-valued function $m_{2,d}$ such that:

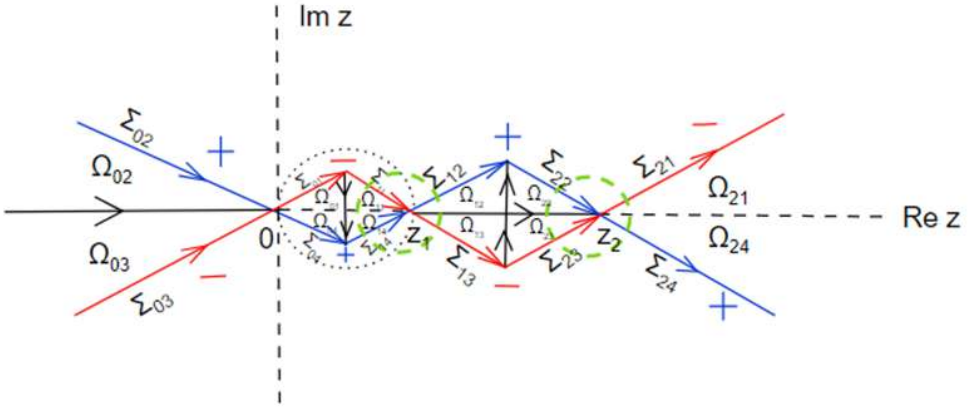
1. $m_{2,d}$ is analytic in $\mathbb{C} \setminus \Sigma'$, where

$$\Sigma' = \Sigma \cup \bigcup_{j=1}^6 \sigma_j \cup \bigcup_{j=1}^6 \sigma'_j, \quad \Sigma = (-\infty, 0) \cup (z_1, z_2) \cup \bigcup_{j=1}^4 \Sigma_{0j} \cup \bigcup_{j=1}^4 \hat{\Sigma}_{1j} \cup \bigcup_{j=1}^4 \hat{\Sigma}_{2j} \quad (3.49)$$

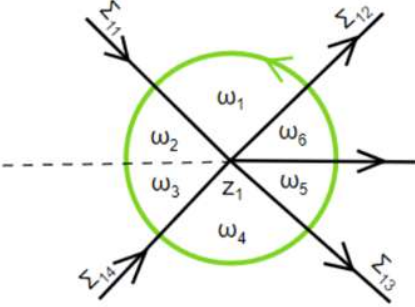
2. $m_{2,d}$ satisfies the jump relation across Σ'

$$m_{2,d+}(z) = m_{2,d-}(z)G_{m_{2,d}}(\xi, z), \quad z \in \Sigma' \quad (3.50a)$$

a



b



c

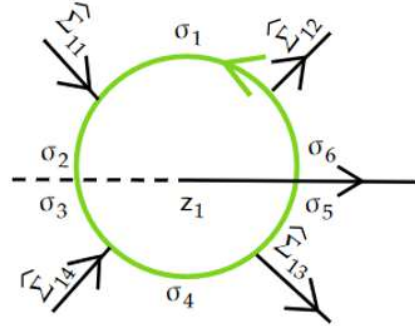


Figure 5: Panel a: circles introduced to avoid the singularities of $\hat{\Delta}$ at the two stationary phase points. Panel b: new regions of non-analyticity for the function $m_{2,d}$ near z_1 . Panel c: jump contours for $m_{2,d}$ near z_1 .

where the jump matrix $G_{m_{2,d}}$ is given by

$$G_{m_{2,d}}(\xi, z) = \begin{cases} U^{-1}(\xi, z)\hat{\Delta}(z), & z \in \sigma_1 \cup \sigma'_1 \\ P(\xi, z)U^{-1}(\xi, z)\hat{\Delta}(z), & z \in \sigma_2 \cup \sigma_3 \cup \sigma'_5 \cup \sigma'_6 \\ M(\xi, z)P(\xi, z)U^{-1}(\xi, z)\hat{\Delta}(z), & z \in \sigma_4 \cup \sigma'_4 \\ D(z)\hat{\Delta}(z), & z \in \sigma_5 \cup \sigma'_3 \\ \hat{\Delta}(z), & z \in \sigma_6 \cup \sigma'_2 \\ D(z), & z \in (-\infty, 0) \cup (z_1, z_2) \end{cases} \quad (3.50b)$$

and the jumps across the segments Σ_{0j} , for $j = 1, \dots, 4$, and $\hat{\Sigma}_{kj}$, for $k = 1, 2$ and $j = 1, \dots, 4$ are the same as the jumps for the function $m_{1,d}$. Here $\hat{\Sigma}_{kj}$ denote the portions of the segments Σ_{kj} which lie outside the circular regions ω_j and ω'_j . Notice that $m_{2,d}$ is analytic inside the circular regions.

3. $m_{2,d}(z) = I_2 + O(1/z)$, $z \rightarrow \infty$

4. The non-tangential limits of $m_{2,d}(z)$ as $z \rightarrow 0$ from \mathbb{C}^\pm exist, and $m_{2,d+}(0) = m_{2,d-}(0) =: m_{2,d}(0)$.

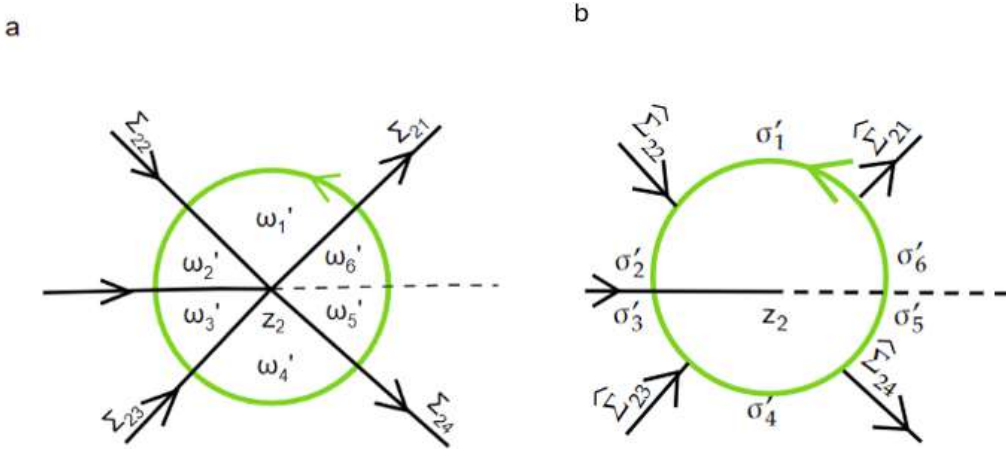


Figure 6: Panel a: new regions of non-analyticity for the function $m_{2,d}$ near z_2 . Panel b: jump contours for $m_{2,d}$ near z_2 .

Finally, we define the function

$$m_{3,d}(z) = m_{2,d}(z)\hat{\Delta}^{-1}(z) \quad (3.51)$$

where

$$\hat{\Delta}(z) = \text{diag}\left(\hat{\delta}(z), 1/\hat{\delta}(z)\right), \quad \hat{\delta}(z) = \exp\left[\frac{1}{2\pi i} \int_{(-\infty, 0) \cup (z_1, z_2)} \frac{\log(1 - |\rho(s)|^2)}{s - z} ds\right] \quad (3.52)$$

and $\hat{\delta}$ satisfies the following scalar RHP.

RHP 9 (RHP for $\hat{\delta}(z)$). *Find a scalar function $\hat{\delta}$ such that:*

1. $\hat{\delta}(z)$ is analytic in $\mathbb{C} \setminus (-\infty, 0) \cup (z_1, z_2)$
2. $\hat{\delta}(z)$ satisfies the jump relation

$$\hat{\delta}_+(z) = \hat{\delta}_-(z) \left(1 - |\rho(z)|^2\right), \quad z \in (-\infty, 0) \cup (z_1, z_2) \quad (3.53)$$

3. $\hat{\delta}(z) = 1 + O(1/z)$, $z \rightarrow \infty$
4. $\hat{\delta}(z)$ has the following asymptotic behavior as $z \rightarrow \mp 1$:

$$\hat{\delta}(z)|z \pm 1|^{-1} = O(1), \quad z \rightarrow \mp 1, \quad z \in \mathbb{C}^+ \quad (3.54a)$$

$$\hat{\delta}(z)|z \pm 1| = O(1), \quad z \rightarrow \mp 1, \quad z \in \mathbb{C}^- \quad (3.54b)$$

In light of RHP 9 and definition (3.51), the function $m_{3,d}$ satisfies the following RHP.

RHP 10 (RHP for $m_{3,d}$). *Find a 2×2 matrix-valued function $m_{3,d}$ such that:*

1. $m_{3,d}$ is analytic in $\mathbb{C} \setminus \Sigma''$, where

$$\Sigma'' = \bigcup_{j=1}^6 \sigma_j \cup \bigcup_{j=1}^6 \sigma'_j \cup \bigcup_{j=1}^4 \Sigma_{0j} \cup \bigcup_{j=1}^4 \hat{\Sigma}_{1j} \cup \bigcup_{j=1}^4 \hat{\Sigma}_{2j}$$

2. $m_{3,d}$ satisfies the jump relation across Σ''

$$m_{3,d+}(z) = m_{3,d-}(z)G_{m_{3,d}}(\xi, z), \quad z \in \Sigma'' \quad (3.55a)$$

where the jump matrix $G_{m_{3,d}}$ is given by

$$G_{m_{3,d}}(\xi, z) = \begin{cases} \hat{\Delta}(z)P(\xi, z)\hat{\Delta}^{-1}(z), & z \in \Sigma_{01} \cup \hat{\Sigma}_{11} \cup \hat{\Sigma}_{21} \\ \hat{\Delta}(z)U(\xi, z)\hat{\Delta}^{-1}(z), & z \in \Sigma_{02} \cup \hat{\Sigma}_{12} \cup \hat{\Sigma}_{22} \\ \hat{\Delta}(z)L(\xi, z)\hat{\Delta}^{-1}(z), & z \in \Sigma_{03} \cup \hat{\Sigma}_{13} \cup \hat{\Sigma}_{23} \\ \hat{\Delta}(z)M(\xi, z)\hat{\Delta}^{-1}(z), & z \in \Sigma_{04} \cup \hat{\Sigma}_{14} \cup \hat{\Sigma}_{24} \\ \hat{\Delta}(z)U^{-1}(\xi, z), & z \in \sigma_1 \cup \sigma'_1 \\ \hat{\Delta}(z)P(\xi, z)U^{-1}(\xi, z), & z \in \sigma_2 \cup \sigma_3 \cup \sigma'_5 \cup \sigma'_6 \\ \hat{\Delta}(z)M(\xi, z)P(\xi, z)U^{-1}(\xi, z), & z \in \sigma_4 \cup \sigma'_4 \\ \hat{\Delta}(z)D(z), & z \in \sigma_5 \cup \sigma'_3 \\ \hat{\Delta}(z), & z \in \sigma_6 \cup \sigma'_2 \end{cases} \quad (3.55b)$$

where again by $\hat{\Sigma}_{kj}$, for $k = 1, 2$ and $j = 1, \dots, 4$ we denote the portions of the segments Σ_{kj} which lie outside the circular regions ω_j and ω'_j .

3. $m_{3,d}(z) = I_2 + \mathcal{O}(1/z)$, $z \rightarrow \infty$

4. The non-tangential limits of $m_{3,d}(z)$ as $z \rightarrow 0$ from \mathbb{C}^\pm exist, and $m_{3,d+}(0) = m_{3,d-}(0) =: m_{3,d}(0)$.

Like in the solitonic region, using the above deformations we can compute $m_{3,d}$ numerically for any $z \in \mathbb{C}$. To obtain m , we still use Eq. (3.36) where $m_{2,d}$ is now replaced by $m_{3,d}$. Finally, the potential $q(x, t)$, is recovered by means of (3.37), where again we replace $m_{2,d}$ by $m_{3,d}$.

Remark 6. Note that the jump matrix D of the function $m_{2,d}$ across $(-\infty, 0) \cup (z_1, z_2)$ becomes singular at $z = \pm 1$, again due to the fact that $\rho(\pm 1) = \mp i$. However, the analog of Proposition 2 can be established in the solitonless region to justify that the boundary values of $m_{3,d}$ are bounded at $z = \pm 1$.

Remark 7. In performing the deformations depicted in Fig. 6 two things are important: (i) the angle at which the black contours leave the circle and (ii) the radius of the circle. For a generic second-order stationary phase point, the second derivative of the phase function $\Theta(z)$ is non-zero, and these contours should all be separated by angles of $\pi/2$, making angles of $\pi/4$ with the real axis, in order to match the local path of steepest descent. Then concerning (ii), this means that the circle intersects the path of the steepest ascent and we may have growth on the circle. To counteract this, we choose the radius proportional to $1/\sqrt{|\Theta''(z_j)|}$ where z_j is the stationary phase point under consideration. This is feasible because while δ has a singularity inside the circle, it is a bounded singularity — it behaves as $(z - z_j)^{\pm iv}$ for $v > 0$. This scaling is discussed further in Section 4 below. Additionally, in our numerical implementations, we find it more convenient to use squares instead of circles for the local deformations near the stationary phase points.

Remark 8. We now briefly discuss the appropriate deformations for the solitonless region when $\xi > 1$. Similarly to the case $\xi < -1$, we open lenses around the origin and the two stationary phase points, \hat{z}_1 and \hat{z}_2 , creating 12 new regions Ω_{kj} enclosed by the boundaries Σ_{kj} , as shown in Fig. 7. The boundaries Σ_{kj} are now defined as follows:

$$\Sigma_{01} = \hat{z}_2 + e^{i\phi}l_2, \quad \Sigma_{02} = \hat{z}_2 + e^{i(\pi-\phi)}\mathbb{R}^+, \quad \Sigma_{11} = \hat{z}_1 + e^{i(\pi-\phi)}l_2, \quad \Sigma_{12} = \hat{z}_1 + e^{i\phi}l_1 \quad (3.56a)$$

$$\Sigma_{21} = e^{i\phi}\mathbb{R}^+, \quad \Sigma_{22} = e^{i(\pi-\phi)}l_1 \quad (3.56b)$$

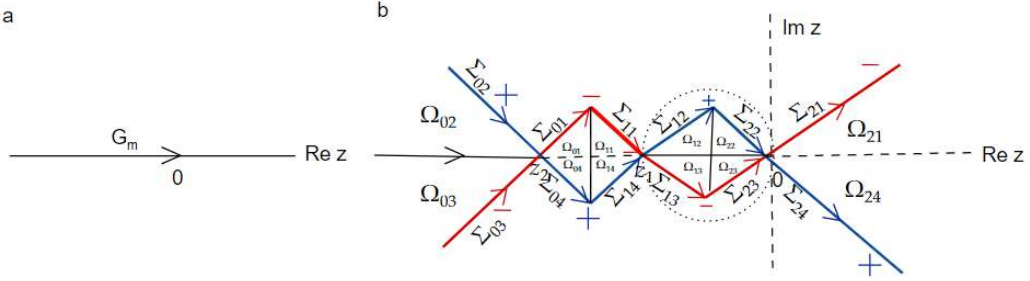


Figure 7: Panel a: the initial jump for the function m . Panel b: the new jump contours after we open lenses in the solitonless region when $\xi > 1$, and the sign of $\text{Re}(i\Theta)$, where $+$ indicates the real part $\text{Re}(i\Theta) > 0$ in the corresponding regions, and $-$ stands for $\text{Re}(i\Theta) < 0$.

$$\Sigma_{k4} = \Sigma_{k1}^*, \quad \Sigma_{k3} = \Sigma_{k2}^*, \quad k = 0, 1, 2 \quad (3.56c)$$

and the real intervals l_1 and l_2 are still given by equation (3.43). Based on panel (c) in Fig. 2, the equations (3.45) also hold in this case, suggesting the use of the LDU factorization for the jump matrix G_m in the regions Ω_{kj} , for $k = 0, 1, 2$ and $j = 2, 3$, and the PM factorization in the regions Ω_{kj} , for $k = 0, 1, 2$ and $j = 1, 4$. Consequently, the definition of the first deformation $m_{1,d}$ is identical to (3.46), and it satisfies the same RHP 7 with the contour of non-analyticity now given by $\Sigma = (-\infty, \hat{z}_2) \cup (\hat{z}_1, 0) \cup \bigcup_{k=0}^2 \bigcup_{j=1}^4 \Sigma_{kj}$. Thus, the jump matrix $D(z)$ is across the contour $(-\infty, \hat{z}_2) \cup (\hat{z}_1, 0)$. To eliminate the jump $D(z)$ in this case, we define

$$\check{\Delta}(z) = \text{diag}\left(\check{\delta}(z), 1/\check{\delta}(z)\right), \quad \check{\delta}(z) = \exp\left[\frac{1}{2\pi i} \int_{(-\infty, \hat{z}_2) \cup (\hat{z}_1, 0)} \frac{\log(1 - |\rho(s)|^2)}{s - z} ds\right]. \quad (3.57)$$

The second deformation $m_{2,d}$ is defined as in Eq. (3.48), except that in this case $\hat{\Delta}(z)$ is replaced by $\check{\Delta}(z)$, ω_j 's are the new circular regions of non-analyticity of $m_{2,d}$ near \hat{z}_1 and ω'_j 's are the new circular regions of non-analyticity of $m_{2,d}$ near \hat{z}_2 , for $j = 1 \cdots 4$. The function $m_{2,d}$ satisfies an RHP similar to 8 where Σ is now replaced by

$$\Sigma = (-\infty, \hat{z}_2) \cup (\hat{z}_1, 0) \cup \bigcup_{j=1}^4 \hat{\Sigma}_{0j} \cup \bigcup_{j=1}^4 \hat{\Sigma}_{1j} \cup \bigcup_{j=1}^4 \Sigma_{2j}$$

and again $\hat{\Sigma}_{kj}$ denote the portions of the segments Σ_{kj} , for $k = 0, 1$ and $j = 1 \cdots 4$, which lie outside the circular regions ω_j and ω'_j . The jump matrix of $m_{2,d}$ is given by equation (3.50b) where $\hat{\Delta}(z)$ is replaced by $\check{\Delta}(z)$, and $D(z)$ is now a jump across $(-\infty, \hat{z}_2) \cup (\hat{z}_1, 0)$. Notice that $m_{2,d}$ is analytic inside the circular regions. To eliminate the jump $D(z)$ we introduce the function $m_{3,d}$ given by

$$m_{3,d}(z) = m_{2,d}(z) \check{\Delta}^{-1}(z)$$

where $\check{\Delta}(z)$ is as in (3.57).

4. Numerical implementation and demonstration

In this section, we describe the numerical code, discuss the numerical challenges, and provide some plots to illustrate the time evolution of the IC for the parameters given in (3.18).

A *Mathematica* implementation of the code will be available as electronic supplementary material. To start, we initialize the values $q_o, h, \theta, \alpha, \phi$ as specified in (3.18). Next, we define the reflection

coefficient (3.19) as a function of the uniformization variable z using (3.20). Note that, although we must define numerically the branch cut arising from $\mu = \sqrt{k^2 - h^2}$, as clarified earlier the expression of $\rho(z)$ is independent of the choice of the branch cut for μ .

In both the solitonic and solitonless regions, the goal is to numerically solve the RHP associated to the final transformation, i.e., the RHP associated to the function $m_{2,d}$ in the solitonic region (RHP 6), and RHP 10 for the function $m_{3,d}$ in the solitonless region. For instance, recall that in the solitonic region $m_{2,d}$ satisfies the jump condition

$$m_{2,d+}(z) = m_{2,d-}(z) G_{m_{2,d}}(\xi, z), \quad z \in \Sigma' = \bigcup_{j=1}^4 \Sigma_j \quad (4.1)$$

where $G_{m_{2,d}}$ is given explicitly in Eq. (3.32b). For any (x, t) with $|x| < 2t$, so that $|\xi| < 1$, we write¹

$$m_{2,d}(z) = I_2 + C_{\Sigma'} u(z)$$

for a new unknown matrix-valued function u where we have defined the Cauchy operator

$$C_{\Sigma} u(z) := \frac{1}{2\pi i} \int_{\Sigma} \frac{u(s)}{s - z} ds.$$

We then define the boundary operators

$$C_{\Sigma}^{\pm} u(z) := \lim_{\substack{z' \rightarrow z \\ z' \in \Omega_{z,\pm}}} C_{\Sigma} u(z'),$$

where $\Omega_{z,+}$ (resp., $\Omega_{z,-}$) is a region just to the left (resp., right) of Σ . So, consider the prototypical problem

RHP 11. Find $m(z)$ satisfying

1. $m(z) = I_2 + C_{\Sigma} u(z)$, $u \in L^2(\Sigma)$, and
2. $m^+(z) = m^-(z)G(z)$, $z \in \Gamma$

In substituting the expression $m(z) = I_2 + C_{\Sigma} u(z)$ into the jump condition, using the Plemelj lemma, $C_{\Sigma}^+ - C_{\Sigma}^- = I$, we find the singular integral equation for u

$$u - (C_{\Sigma}^- u)(G - I_2) = G - I_2. \quad (4.2)$$

We then write (4.1) as an integral equation

$$m_{2,d}(z) = I_2 + C_{\Sigma'} u_{2,d}(z), \quad u_{2,d} - (C_{\Sigma'}^- u_{2,d})(G_{m_{2,d}} - I_2) = G_{m_{2,d}} - I_2. \quad (4.3)$$

Similarly, in the solitonless region $m_{2,d}, u_{2,d}$ in (4.3) will be replaced by $m_{3,d}, u_{3,d}$ and Σ' will be replaced by Σ'' .

Singular integral equations like (4.3) are tractable numerically using the method of Olver [27] (see also [32]) provided that the contour Σ' is a union of line segments and the jump matrix $G_{m_{2,d}}$ satisfies some regularity conditions [32]. The method is a Chebyshev collocation method that makes use of an explicit representation of the Cauchy integrals, and their boundary values, of Chebyshev polynomials in terms of special functions, or alternatively, one can use Legendre polynomials and their associated three-term recurrence [28], with special care taken at intersection points.

For the current work, as noted above, we use the two packages RHPackage and ISTPackage which are implemented in Mathematica [26, 30]. These packages provide tools for the convenient input of jump contours and jump matrices. The resulting collocation linear system can then be reliably solved

¹This ansatz can be justified by additional estimates on the Jost solutions, showing that they are in an appropriate Hardy space.

to the desired level of accuracy by monitoring the decay of the Chebyshev coefficients of the resulting approximate solution. We refer the reader to [32] for more details.

The behavior of the solution $m(z)$ at infinity, or at the origin, can be (formally) computed via

$$m(z) = I_2 - \frac{1}{2\pi iz} \int_{\Sigma} u(s) ds + o(z^{-1}), \quad z \rightarrow \infty, \tag{4.4}$$

$$m(z) = I_2 + \frac{1}{2\pi i} \int_{\Sigma} \frac{u(s)}{s} ds + o(1), \quad z \rightarrow 0. \tag{4.5}$$

To justify these expressions, we see that if $G - I_2 \in L^2(\Sigma) \cap L^1(\Sigma)$ then (4.2) implies that $u \in L^1(\Sigma)$ and (4.4) follows. Similarly, when, for simplicity, Σ is a union of line segments, if $G - I_2 \in H^1(\Sigma)$ and $G(0) = I_2$, we have that $m(z)$ takes continuous boundary values in a neighborhood of $z = 0$ and the boundary values are all given by (4.5).

For a visual representation of the time evolution of the IC with the parameters given in (3.18) for small values of x , please refer to Fig. 8. Plots of the solution over larger spatial domains are shown in

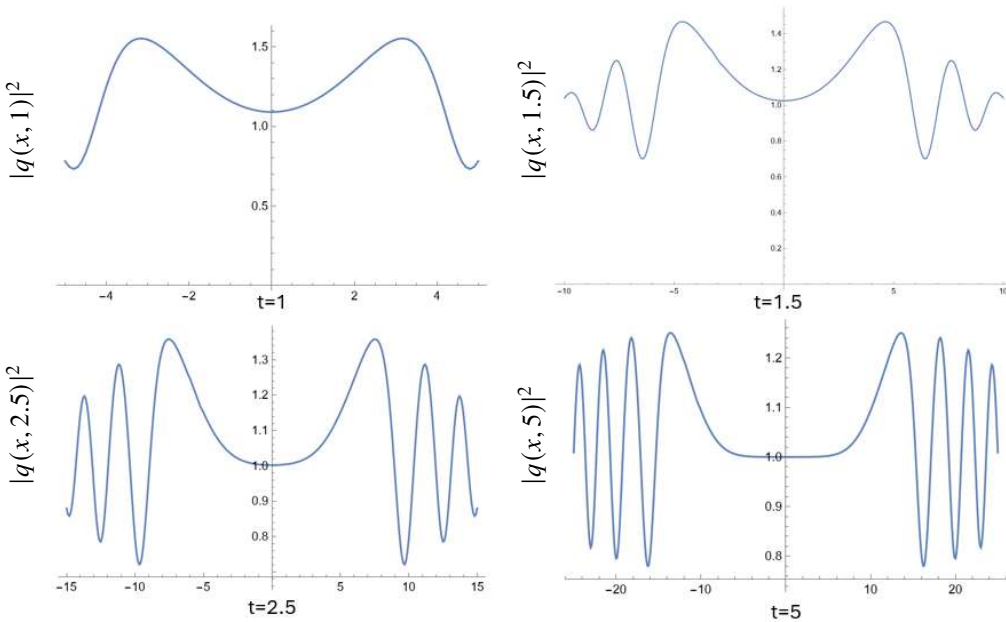


Figure 8: Plot of $|q(x, t)|^2$ for fixed values of t as a function of x for IC as in (1.3), with parameters as in (3.18).

Fig. 1 and 14. In Fig. 9 we plot the solution off into asymptotic regimes to demonstrate the asymptotic effectiveness of the method. In actuality, the numerical method becomes more accurate and efficient for larger values of parameters. This is due to the scaling that is discussed in Remark 7 and described in more detail in [29]. Off into asymptotic regimes, one is left with essentially disconnected, fixed contours that scale as $1/\sqrt{t}$. We demonstrate this in Fig. 9 where we see that as t increases, $x/t = -4$, the contours on which the Riemann–Hilbert problem is (numerically) posed, after scaling, limit to a fixed contour. Behind this limiting configuration is a contour truncation algorithm that prunes both entire contours when the jump matrix is sufficiently close to the identity and shrinks existing contours using the same

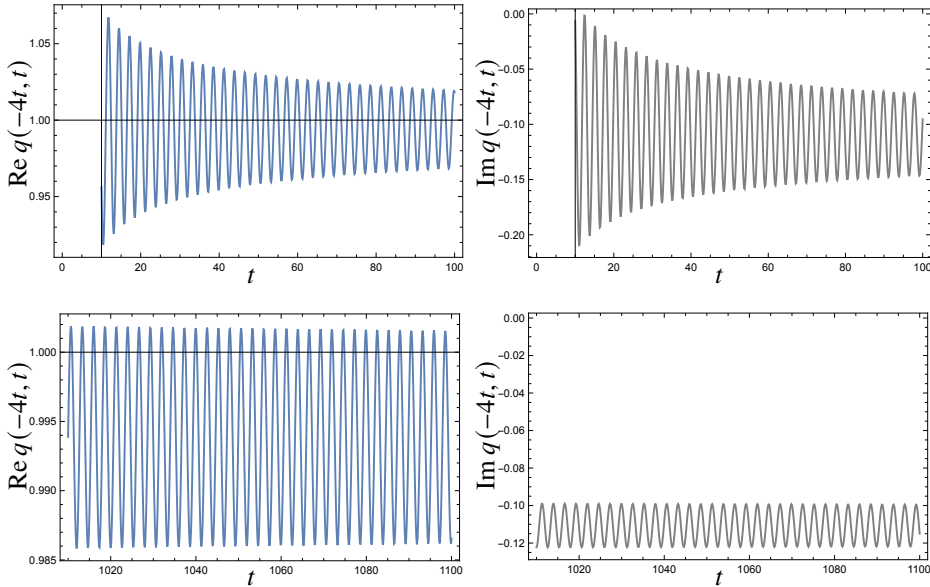


Figure 9: The real (left) and imaginary parts (right) of the solution of the NLS equation with IC (1.3) and parameters as in (3.18) for large values of (x, t) such that $x = -4t$.

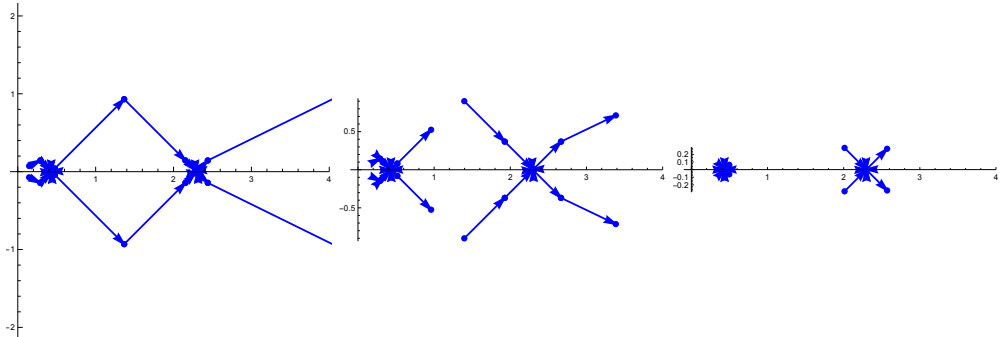


Figure 10: The contours used in the computation of $m_{3,d}$ for $\xi = -2 < -1$ (right-half plane only) for $t = 1, 10, 100$ (left, center, right, respectively).

metric. For the specifics of this method, we refer the reader to [30]. The exact implementation of the contours for $\xi = -2 < -1$ is demonstrated in Fig. 10, 11, 12.

It is crucial to emphasize that the function Δ , which eliminates the jump D in both regions, plays a key role in the definition of the jump matrices for $m_{2,d}$ (or $m_{3,d}$). Consequently, it is essential to define Δ appropriately by computing numerically the relevant Cauchy integrals. We give these details in Appendix B

5. Concluding remarks

In this work, we implemented the numerical IST for the defocusing NLS equation with constant nonzero boundary conditions and a box-type IC at $t = 0$ in order to approximate the solution of the Cauchy problem for $t > 0$. So far, the numerical IST had been implemented in the literature for a number of nonlinear integrable equations always assuming ICs in Schwartz class (i.e., smooth and rapidly decaying to zero). To our knowledge, this is the first work in which the method is generalized to the NLS equation

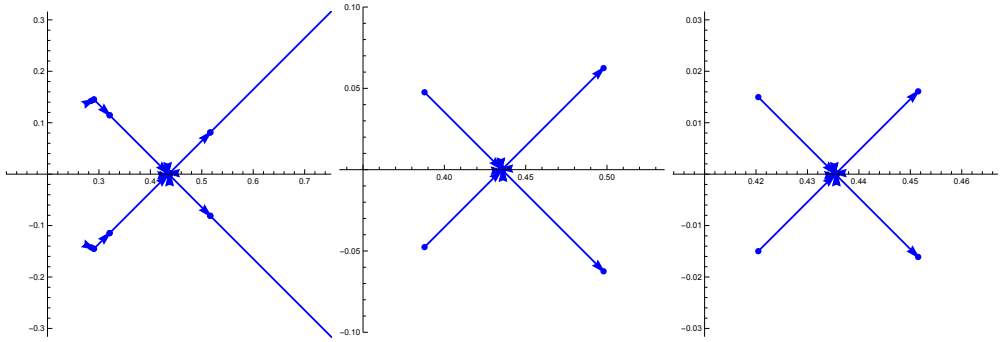


Figure 11: The contours used in the computation of $m_{3,d}$ for $\xi = -2 < -1$ for $t = 10, 100, 1000$ (left, center, right, respectively) near the left-most stationary phase point z_1 . As t increases the contours are scaled and truncated following Remark 7.

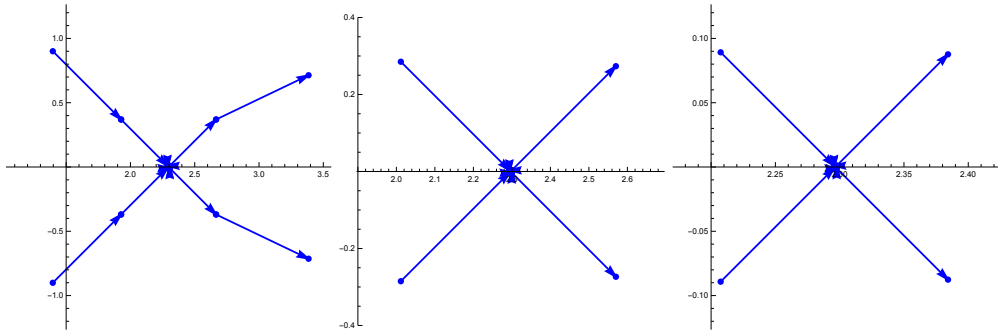


Figure 12: The contours used in the computation of $m_{3,d}$ for $\xi = -2 < -1$ for $t = 10, 100, 1000$ (left, center, right, respectively) near the right-most stationary phase point z_2 . As t increases the contours are scaled and truncated following Remark 7.

with ICs that do not decay rapidly at space infinity and also exhibit a jump discontinuity. Several directions for further exploration remain open. One avenue for future research is the numerical study of the collisionless shock region, which is an open problem also as far as the long-time asymptotics is concerned. Another direction for future investigation is to consider an IC that admits solitons, and solve the associated RHP numerically. Including one or more solitons can also be done following a similar approach as in the rapidly decaying case, which amounts to turning the residue conditions at each discrete eigenvalue into suitable jump conditions, and then implementing the additional required contour deformations. Finally, a natural follow-up problem is the case of a smooth IC decaying sufficiently rapidly to the nonzero background. An advantage here is that the reflection coefficient will have faster decay as $z \rightarrow 0$ and as $z \rightarrow -\infty$, thus simplifying the numerical evaluation of the associated Cauchy integrals. On the other hand, the numerical implementation of the direct problem will be required, which can be done in a similar way as to the case of rapidly decaying ICs. A key challenge will be incorporating the $\bar{\partial}$ -problem into the inverse problem of the IST, since in this case the reflection coefficient does not admit analytic continuation to the entire complex plane. This issue arises from the non-analyticity of the reflection coefficient and represents a novel challenge from a numerical perspective.

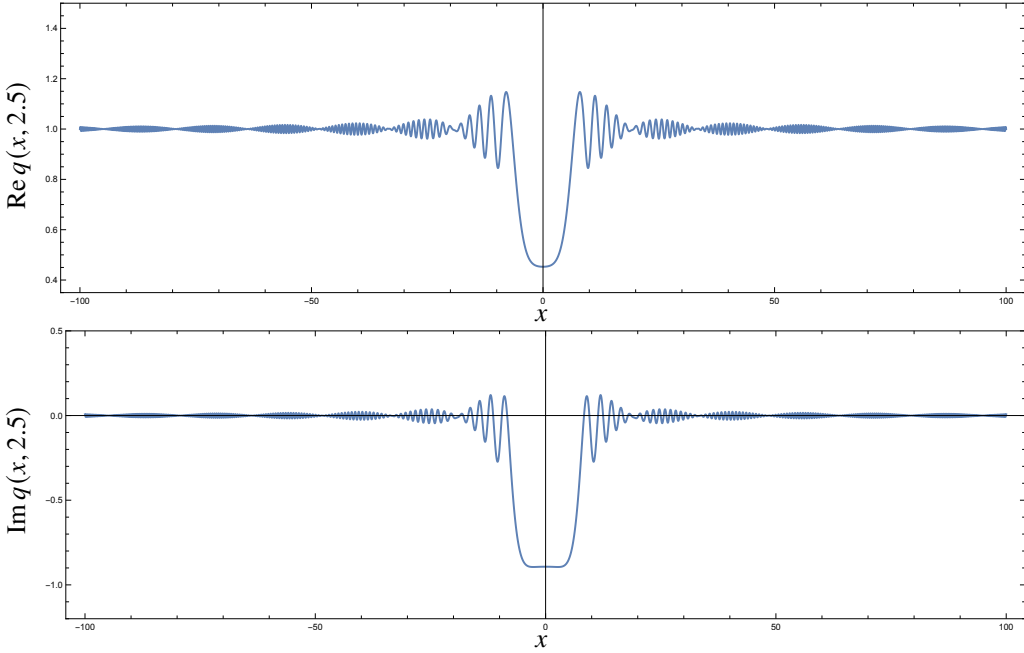


Figure 13: The real (top) and imaginary parts (bottom) of the solution of the NLS equation with IC (1.3) at $t = 2.5$ with parameters as in (3.18).

A. δ in the solitonic region

In this section, we are providing the solution to the RHP 5. Recall that the function δ satisfies the following jump condition

$$\delta_+(z) = \delta_-(z) \left(1 - |\rho(z)|^2\right), \quad z \in (-\infty, 0). \quad (\text{A.1})$$

Applying the Sokhotski–Plemelj formula to this condition yields

$$\begin{aligned} \delta(z) &= \exp\left(\frac{1}{2\pi i} \int_{-\infty}^0 \frac{\log(1 - |\rho(s)|^2)}{s - z} ds\right) \\ &= \exp\left(\frac{1}{2\pi i} \int_{-\infty}^{\gamma_b} \frac{\log(1 - |\rho(s)|^2)}{s - z} ds + \frac{1}{2\pi i} \int_{\gamma_b}^{\gamma} \frac{\log(1 - |\rho(s)|^2)}{s - z} ds + \frac{1}{2\pi i} \int_{\gamma}^0 \frac{\log(1 - |\rho(s)|^2)}{s - z} ds\right), \end{aligned} \quad (\text{A.2})$$

where $\gamma, \gamma_b \in (-\infty, 0)$ with $\gamma_b < -1 < \gamma$. The second integral in (A.2) can be computed numerically using Mathematica-computable special functions. We also show below how the singular part of the integral can be dealt with analytically, following a similar strategy as the one used for the Toda lattice in [4]. Let us define

$$\mathcal{T}(z) = \frac{1}{2\pi i} \int_{\gamma_b}^{\gamma} \frac{\log(1 - |\rho(s)|^2)}{s - z} ds. \quad (\text{A.3})$$

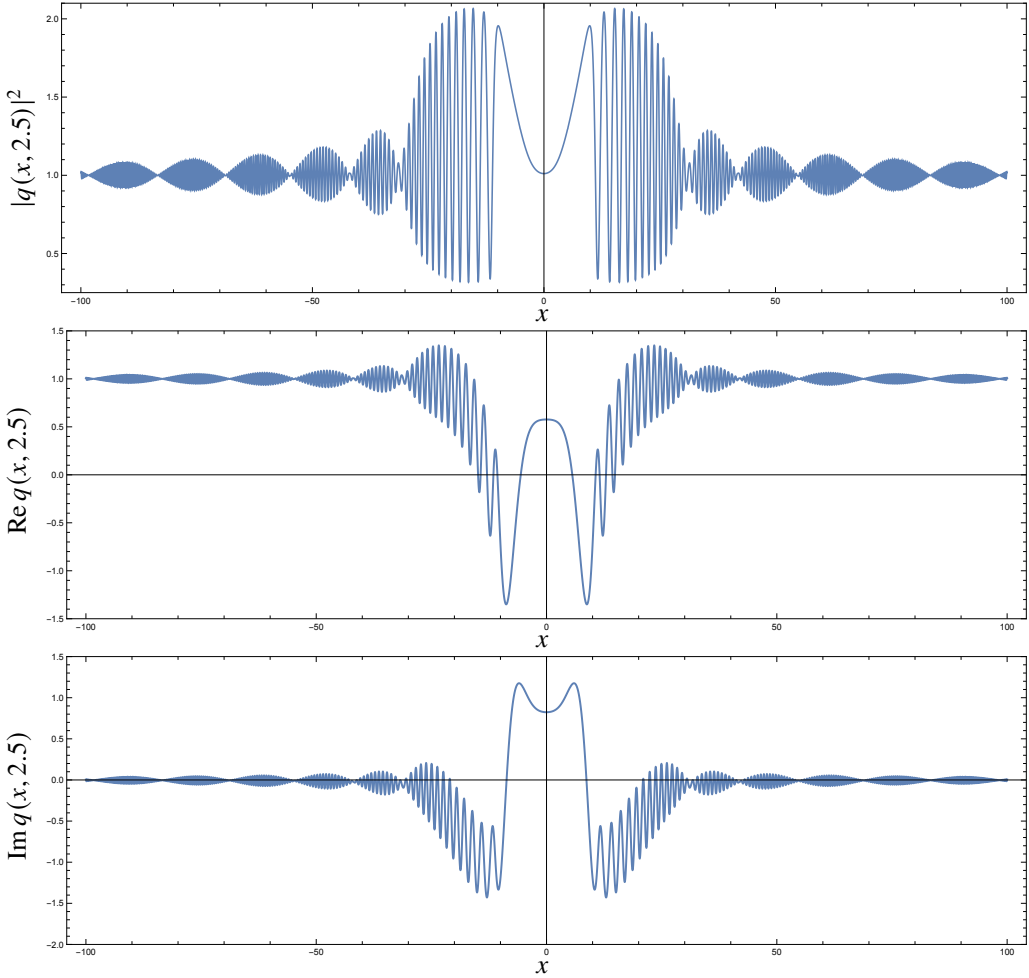


Figure 14: The squared modulus (top), real part (middle) and imaginary part (bottom) of the solution of the NLS equation with IC (1.3) at $t = 2.5$ with parameters as in (3.18) but with $h = 3.0$.

Note that the function $\log(1 - |\rho(z)|^2)$ is singular at $z = -1 \in (\gamma_b, \gamma)$ since $\rho(-1) = i$. We regularize the integrand by introducing the function

$$\tilde{\tau}(z) = \frac{1 - |\rho(z)|^2}{(z - z^{-1})^2} > 0, \quad z \in (\gamma_b, \gamma) \quad (\text{A.4})$$

and rewriting $\mathcal{T}(z)$ as

$$\mathcal{T}(z) = \frac{1}{2\pi i} \int_{\gamma_b}^{\gamma} \frac{\log(\tilde{\tau}(s))}{s - z} ds + \frac{1}{2\pi i} \int_{\gamma_b}^{\gamma} \frac{\log(s - s^{-1})^2}{s - z} ds \quad (\text{A.5})$$

where the function $\log(\tilde{\tau}(z))$ is smooth over (γ_b, γ) . The function $\log(z - z^{-1})^2$ is singular at $z = -1$, but its Cauchy integral

$$\mathcal{T}_1(z) = \frac{1}{2\pi i} \int_{\gamma_b}^{\gamma} \frac{\log(s - s^{-1})^2}{s - z} ds \quad (\text{A.6})$$

can be computed analytically. Indeed, for $z \in (\gamma_b, \gamma)$ we have

$$\log(z - z^{-1})^2 = 2 \log(z + 1) + 2 \log(1 - z^{-1}), \tag{A.7}$$

which yields

$$\mathcal{T}_1(z) = \frac{1}{2\pi i} \int_{\gamma_b}^{\gamma} \frac{2 \log(s + 1)}{s - z} ds + \frac{1}{2\pi i} \int_{\gamma_b}^{\gamma} \frac{2 \log(1 - s^{-1})}{s - z} ds, \tag{A.8}$$

where the function $\log(1 - z^{-1})$ is smooth over (γ_b, γ) . It remains to compute the integral

$$\mathcal{T}_2(z) = \frac{1}{2\pi i} \int_{\gamma_b}^{\gamma} \frac{2 \log(s + 1)}{s - z} ds. \tag{A.9}$$

To deal with the singularity of the function $\log(z + 1)$ at $z = -1$, let us consider a closed curve σ that encircles $z = -1$. We denote by D_σ the region enclosed by σ , and $D_\sigma^c = \mathbb{C} \setminus D_\sigma$. We also choose the branch cut of the function $\log(z + 1)$ to be the line $z + 1 = re^{i\theta}$ with $-\pi/2 \leq \theta \leq \pi/2$. From Cauchy's integral formula (integrating over the closed curve σ), we get

$$\begin{aligned} \mathcal{T}_2(z) \equiv \lim_{\epsilon \rightarrow 0} \left(\frac{1}{2\pi i} \int_{\Gamma_\epsilon} f(s, z) ds \right) &= -\frac{1}{2\pi i} \int_{(\gamma, \gamma_b)_{\text{arc}}} f(s, z) ds - \lim_{\epsilon \rightarrow 0} \left(\frac{1}{2\pi i} \int_{C_\epsilon} f(s, z) ds \right) + \\ &+ \begin{cases} 2 \log(z + 1), & z \in D_\sigma \\ 0, & z \in D_\sigma^c \end{cases} \end{aligned} \tag{A.10}$$

where $(\gamma, \gamma_b)_{\text{arc}}$ denotes the semicircle centered at $z = -1$ with radius $r = \frac{|\gamma - \gamma_b|}{2}$ and counterclockwise orientation, C_ϵ denotes the semicircle centered at $z = -1$ with radius ϵ and counterclockwise orientation, $\Gamma_\epsilon = [\gamma_b, \gamma] \setminus C_\epsilon$, and we introduced the notation $f(s, z)$ for the function $2 \log(s + 1)/(s - z)$ for brevity. One can show that there exists K_ϵ such that $|(s + 1)f(s, z)| \leq K_\epsilon$, where K_ϵ depends on ϵ but not on the argument $\arg(s + 1)$, and therefore $(s + 1)f(s, z)$ approaches zero uniformly as $\epsilon \rightarrow 0$, which implies that

$$\lim_{\epsilon \rightarrow 0} \left(\frac{1}{2\pi i} \int_{C_\epsilon} f(s, z) ds \right) = 0. \tag{A.11}$$

Moreover, it turns out that

$$\frac{1}{2\pi i} \int_{(\gamma, \gamma_b)_{\text{arc}}} f(s, z) ds = \frac{1}{\pi i} \left(\log r \log \frac{z + 1 - r}{1 + z} - \log(-r) \log \frac{z + 1 + r}{1 + z} - \text{Li}_2\left(\frac{-r}{1 + z}\right) + \text{Li}_2\left(\frac{r}{1 + z}\right) \right), \tag{A.12}$$

where Li_2 is the dilogarithm function. Combining all the above into (A.10) we get

$$\begin{aligned} \mathcal{T}_2(z) &= -\frac{1}{\pi i} \left(\log r \log \frac{z + 1 - r}{1 + z} - \log(-r) \log \frac{z + 1 + r}{1 + z} - \text{Li}_2\left(\frac{-r}{1 + z}\right) + \text{Li}_2\left(\frac{r}{1 + z}\right) \right) + \\ &+ \begin{cases} 2 \log(z + 1), & z \in D_\sigma \\ 0, & z \in D_\sigma^c \end{cases}. \end{aligned} \tag{A.13}$$

B. Computing δ

We give below some details regarding the numerical evaluation of these integrals. Recall that in the solitonic region $\Delta(z) = \text{diag}(\delta(z), 1/\delta(z))$, where δ is given by the expression

$$\delta(z) = \exp \left[\frac{1}{2\pi i} \int_{-\infty}^0 \frac{\log(1 - |\rho(s)|^2)}{s - z} ds \right]. \quad (\text{B.1})$$

Moreover, recall that the reflection coefficient is such that $\rho(\pm 1) = \mp i$, which makes the function $\log(1 - |\rho(s)|^2)$ singular at $s = -1$. We then rewrite δ as follows

$$\delta(z) = \exp \left[\frac{1}{2\pi i} \left(\int_{-\infty}^{\gamma_b} \frac{\log(1 - |\rho(s)|^2)}{s - z} ds + \int_{\gamma_b}^{\gamma} \frac{\log(1 - |\rho(s)|^2)}{s - z} ds + \int_{\gamma}^0 \frac{\log(1 - |\rho(s)|^2)}{s - z} ds \right) \right] \quad (\text{B.2})$$

where $\gamma, \gamma_b \in (-\infty, 0)$ with $\gamma_b < -1 < \gamma$. Notice that the function $\log(1 - |\rho(s)|^2)$ is regular inside $(-\infty, \gamma_b)$ and $(\gamma, 0)$, and is singular inside the interval (γ_b, γ) . The main challenge in numerically evaluating the first Cauchy integral in Eq. (B.2) lies in the slow decay of the reflection coefficient as $z \rightarrow -\infty$. Conversely, the difficulty with the third Cauchy integral in (B.2) is given by the fast oscillations of the reflection coefficient near zero. To address these issues, we truncated the Cauchy integrals to the left of $z = 0$ and to the right of $z \rightarrow -\infty$ enabling us to achieve high accuracy while managing computational costs effectively. We then use a Chebyshev approximation for the function $\log(1 - |\rho(s)|^2)$ as it remains smooth within the integration interval. The Cauchy integrals are then computed using Mathematica's special functions that define numerically the Cauchy transform. For the second integral in (B.2), the function $\log(1 - |\rho(s)|^2)$ is singular at $s = -1$. We therefore rewrite this integral as follows

$$\int_{\gamma_b}^{\gamma} \frac{\log(1 - |\rho(s)|^2)}{s - z} ds = \int_{\gamma_b}^{\gamma} \log \left(\frac{1 - |\rho(s)|^2}{(s+1)^2} \right) \frac{1}{s - z} ds + \int_{\gamma_b}^{\gamma} \frac{\log((s+1)^2)}{s - z} ds \quad (\text{B.3})$$

where the function $\log \left(\frac{1 - |\rho(s)|^2}{(s+1)^2} \right)$ is smooth along (γ_b, γ) and its Cauchy integral can be computed using a Chebyshev approximation. The function $\log((s+1)^2)$ is still singular at $s = -1$. However, we can derive a closed-form expression for its Cauchy integral using special function routines in Mathematica. On the other hand, in the solitonless region when $\xi < -1$, $\hat{\Delta}(z) = \text{diag}(\hat{\delta}(z), 1/\hat{\delta}(z))$ where $\hat{\delta}$ is given by the expression

$$\hat{\delta}(z) = \exp \left[\frac{1}{2\pi i} \int_{-\infty}^0 \frac{\log(1 - |\rho(s)|^2)}{s - z} ds + \frac{1}{2\pi i} \int_{z_1}^{z_2} \frac{\log(1 - |\rho(s)|^2)}{s - z} ds \right] \quad (\text{B.4})$$

where $z_1 < 1 < z_2$. The function $\log(1 - |\rho(s)|^2)$ now becomes singular at $s = \pm 1$. $\hat{\delta}$ is defined exactly the same way as in the solitonic region when $s \in (-\infty, 0)$. When $s \in (z_1, z_2)$, we rewrite the second integral in Eq. (B.4) as follows

$$\frac{1}{2\pi i} \int_{z_1}^{\gamma'_b} \frac{\log(1 - |\rho(s)|^2)}{s - z} ds + \frac{1}{2\pi i} \int_{\gamma'_b}^{\gamma'} \frac{\log(1 - |\rho(s)|^2)}{s - z} ds + \frac{1}{2\pi i} \int_{\gamma'}^{z_2} \frac{\log(1 - |\rho(s)|^2)}{s - z} ds \quad (\text{B.5})$$

with $z_1 < \gamma'_b < \gamma' < z_2$. The function $\log(1 - |\rho(s)|^2)$ is smooth along $(z_1, \gamma'_b) \cup (\gamma', z_2)$, and the corresponding Cauchy integrals can be computed numerically using a Chebyshev approximation. To

deal with the singularity at $s = 1$, we write

$$\frac{1}{2\pi i} \int_{\gamma'_b}^{\gamma'} \frac{\log(1 - |\rho(s)|^2)}{s - z} ds = \int_{\gamma'_b}^{\gamma'} \log\left(\frac{1 - |\rho(s)|^2}{(s - 1)^2}\right) \frac{1}{s - z} ds + \int_{\gamma'_b}^{\gamma'} \frac{\log((s - 1)^2)}{s - z} ds \quad (\text{B.6})$$

where the function $\log\left(\frac{1 - |\rho(s)|^2}{(s - 1)^2}\right)$ is smooth along (γ'_b, γ') and its Cauchy integral can be computed using a Chebyshev approximation. The function $\log((s - 1)^2)$ is still singular at $s = 1$, but its Cauchy integral can be computed using special function routines in Mathematica. Moreover, in the solitonless region when $\xi > 1$, we define $\hat{\Delta}(z) = \text{diag}(\hat{\delta}(z), 1/\hat{\delta}(z))$ where $\hat{\delta}$ is given by the expression

$$\hat{\delta}(z) = \exp\left[\frac{1}{2\pi i} \int_{-\infty}^{z_2} \frac{\log(1 - |\rho(s)|^2)}{s - z} ds + \frac{1}{2\pi i} \int_{z_1}^0 \frac{\log(1 - |\rho(s)|^2)}{s - z} ds\right]. \quad (\text{B.7})$$

Note that since $z_2 < -1 < z_1 < 0$, the values $s = \pm 1$ do not lie on the contour of integration. Therefore, the function $\log(1 - |\rho(s)|^2)$ is smooth along the contour $(-\infty, z_2) \cup (z_1, 0)$, and its Cauchy integral can be computed numerically using a Chebyshev approximation. As before, we truncate the first Cauchy integral in (B.7) to the right of $z \rightarrow -\infty$ and the second integral to the left of $z = 0$, in order to account for the slow decay and fast oscillations of the reflection coefficient at $-\infty$ and at 0, respectively. From a numerical perspective, the definition of $\hat{\delta}$ is simpler in the solitonless region when $\xi > 1$ compared to the same region when $\xi < -1$, where as we saw earlier, the singularities of the function $\log(1 - |\rho(s)|^2)$ at $s = \pm 1$ must be accounted for.

Acknowledgments. A.G. and B.P. would like to thank Ken McLaughlin for many insightful discussions, as well as the Isaac Newton Institute for Mathematical Sciences, Cambridge, for support and hospitality during the satellite programme “Emergent phenomena in nonlinear dispersive waves” (supported by EPSRC grant EP/R014604/1), where work on this paper was undertaken.

Funding Statement. B.P. and T.T. acknowledge partial support for this research through grants from the National Science Foundation DMS-2406626 and DMS-2306438, respectively.

Competing Interests. None.

Data Availability Statement. The code used to produce the figures in this paper will be available in the electronic supplementary materials.

Ethical Standards. The research meets all ethical guidelines.

Author Contributions. Conceptualization: A.G.; B.P.; T.T. Methodology: A.G.; B.P.; T.T. Writing original draft: A.G.; B.P.; T.T. All authors approved the final submitted draft.

References

- [1] D. Bilman and P. Miller, “A Robust Inverse Scattering Transform for the Focusing Nonlinear Schrödinger Equation”. *Comm. Pure App. Math.* LXXII, 1722–1805 (2019).
- [2] D. Bilman, P. Nabelek, and T. Trogdon (2023). “Computation of large-genus solutions of the Korteweg–de Vries equation”. *Physica D: Nonlinear Phenomena*, **449**, 133715 (2023).
- [3] D. Bilman and T. Trogdon, “On numerical inverse scattering for the Korteweg-de Vries equation with discontinuous step-like data”, *Nonlinearity*, **33** (5), 2211–2269 (2020).
- [4] D. Bilman and T. Trogdon, “Numerical Inverse Scattering for the Toda lattice”. *Comm. Math. Phys.* **352**, 805–879 (2017).
- [5] G. Biondini and B. Prinari, “On the spectrum of the Dirac operator and the existence of discrete eigenvalues for the defocusing nonlinear Schrödinger equation”. *Stud. App. Math.* **132**(2), 138–159 (2014).
- [6] S. Cuccagna and R. Jenkins, “On the asymptotic stability of N -soliton solutions of the defocusing nonlinear Schrödinger equation”. *Comm. Math. Phys.* **343**(3), 921–969 (2016).
- [7] P. Deift, A. Its and X. Zhou, “Long-time asymptotics for integrable nonlinear wave equations”. *Important Developments in Soliton Theory*, Springer Ser. Nonlin. Dyn., pp. 181–204 (Springer, Berlin 1993).

- [8] P. Deift, S. Venakides and X. Zhou, “New results in small dispersion KdV by an extension of the steepest descent method for Riemann–Hilbert problems”. IMRN: International Mathematics Research Notices, 1997.6 (1997).
- [9] P. Deift and X. Zhou, “A steepest descent method for oscillatory Riemann–Hilbert problems. Asymptotics for the MKdV equation”. *Ann. Math.* **137** 295–368, 1993.
- [10] P. Deift and X. Zhou, “Long-time asymptotics for integrable systems. Higher order theory”. *Comment. Phys. Math.* **165**, 175–191 (1994).
- [11] P. Deift and X. Zhou, “Long-Time Behavior of the Non-Focusing Nonlinear Schrödinger Equation, a Case Study”. *Lectures in Mathematical Sciences*, New Ser., vol. 5, Graduate School of Mathematical Sciences, University of Tokyo, p. 61 (1994).
- [12] P. Deift and X. Zhou, “Long-time asymptotics for solutions of the NLS equation with initial data in a weighted Sobolev space”. *Commun. Pure Appl. Math.* **56**, 1029–1077 (2003).
- [13] P. Deift, X. Zhou and S. Venakides, “An extension of the steepest descent method for Riemann–Hilbert problems: the small dispersion limit of the Korteweg–de Vries equation”. *Proc. Natl. Acad. Sci.* **95**(2), 445–454 (1998).
- [14] F. Demontis, B. Prinari, C. van der Mee and F. Vitale, “The inverse scattering transform for the defocusing nonlinear Schrödinger equation with nonzero boundary conditions”. *Stud. App. Math.* **131**, 1–40 (2013).
- [15] M. Dieng, and K. McLaughlin, “Long-time asymptotics for the NLS equation via \bar{d} bar methods”. arXiv:0805.2807 (2008).
- [16] J.C. DiFranco and K.T.-R. McLaughlin, “A nonlinear Gibbs-type phenomenon for the defocusing nonlinear Schrödinger equation”. *IMRP Int. Math. Res. Pap.* **2005**, pp. 403–549 (2005).
- [17] L. D. Faddeev and L. A. Takhtajan, *Hamiltonian methods in the theory of solitons* (Springer, Berlin, 1987).
- [18] B. Fornberg and N. Flyer, “A numerical implementation of Fokas boundary integral approach: Laplace’s equation on a polygonal domain”. *Royal Society Proc Series A* **467**, 2983–3003 (2011).
- [19] C. Gallo, “Schrödinger group on Zhidkov spaces”. *Adv. Diff. Eqs.* **9**, 509–538 (2004).
- [20] C. Gallo, “The Cauchy problem for defocusing nonlinear Schrödinger equations with non-vanishing initial data at infinity”. *Commun. Partial Differ. Equ.* **33**, 729–771 (2008).
- [21] A.-K. Kassam and L.N. Trefethen, “Fourth-order time-stepping for stiff PDEs”. *SIAM J. Sci. Comput.* **26**, 1214–1233 (2005).
- [22] C. Klein, “Fourth order time-stepping for low dispersion Korteweg-de Vries and nonlinear Schrödinger equations”. *Electron. Trans. Numer. Anal.* **29**, 116–135 (2008).
- [23] A. Liu and T. Trogdon, “An artificially-damped Fourier method for dispersive evolution equations”. *App. Num. Math.* **192**, 19–40 (2023).
- [24] K.T.-R. McLaughlin and P.D. Miller, “The $\bar{\delta}$ steepest descent method and the asymptotic behavior of polynomials orthogonal on the unit circle with fixed and exponentially varying nonanalytic weights”. *IMRP Int. Math. Res. Pap.* (2006), Art. ID 48673, 1–77 (2006).
- [25] K.T.-R. McLaughlin and P.D. Miller, “The $\bar{\delta}$ steepest descent method for orthogonal polynomials on the real line with varying weights”. *Int. Math. Res. Not. IMRN*, Art. ID rnn 075, 66 pp (2008).
- [26] S. Olver, RHPackage, <https://github.com/dlfivefifty/RHPackage> (2010).
- [27] S. Olver, “A general framework for solving Riemann–Hilbert problems numerically”. *Numer. Math.* **122**, 305–340 (2012).
- [28] S. Olver, R.M. Slevinsky and A. Townsend, “Fast algorithms using orthogonal polynomials”. *Acta Numerica* **29**, 573–699 (2020).
- [29] S. Olver and T. Trogdon, “Nonlinear steepest descent and the numerical solution of Riemann–Hilbert problems”. *Comm. Pure Appl. Math.* **67**, 1353–1389 (2014).
- [30] T. Trogdon, ISTPackage, <https://bitbucket.org/trogdon/istpackage> (2013).
- [31] T. Trogdon and S. Olver, “Numerical inverse scattering for the focusing and defocusing nonlinear Schrödinger equations”. *Proc. Roy. Soc. Lon. A* **469**, 20120330 (2013).
- [32] T. Trogdon and S. Olver, *Riemann–Hilbert Problems, Their Numerical Solution, and the Computation of Nonlinear Special Functions* (SIAM, Philadelphia, 2015).
- [33] T. Trogdon, S. Olver and B. Deconinck, “Numerical inverse scattering for the Korteweg–de Vries and modified Korteweg–de Vries equations”. *Physica D* **241**, 1003–1025 (2012).
- [34] A.H. Vartanian, “Long-time asymptotics of solutions to the Cauchy problem for the defocusing nonlinear Schrödinger equation with finite-density initial data. I. Solitonless sector”. In: *Recent developments in integrable systems and Riemann–Hilbert problems* (Birmingham, AL, 2000), pp. 91–185. *Contemp. Math.*, vol. 326. Amer. Math. Soc., Providence (2003).
- [35] A.H. Vartanian, “Long-time asymptotics of solutions to the Cauchy problem for the defocusing nonlinear Schrödinger equation with finite-density initial data. II. Dark solitons on continua”. *Math. Phys. Anal. Geom.* **5**, 319–413 (2002).
- [36] A.H. Vartanian, “Exponentially small asymptotics of solutions to the defocusing nonlinear Schrödinger equation”. *Appl. Math. Lett.* **16**, 425–434 (2003).
- [37] W. Zhaoyu and E. Fan, “Defocusing NLS equation with nonzero background: Large-time asymptotics in a solitonless region”. *J. Differ. Equ.* **336**, 334–373 (2022).
- [38] X. Zhou, “ L^2 -Sobolev space bijectivity of the scattering and inverse scattering transforms”, *Commun. Pure Appl. Math.* **51**, 697–731 (1998).